Mapping arginase expression with ^{18}F-fluorinated late-generation arginase inhibitors derived from quaternary α-amino acids

Gonçalo S. Clemente[1], Inês. F. Antunes[1], Santosh Kurhade[2], Mariska P. M. van den Berg[3], Jürgen W. A. Sijbesma[1], Aren van Waarde[1], Rogier C. Buijsman[4], Nicole Willemsen-Seegers[4], Reinoud Gosens[3], Herman Meurs[3], Alexander Dömling[2], and Philip H. Elsinga[1]

[1]Department of Nuclear Medicine and Molecular Imaging – University Medical Center Groningen, University of Groningen, The Netherlands; [2]Department of Drug Design, University of Groningen, The Netherlands; [3]Department of Molecular Pharmacology, University of Groningen, The Netherlands; [4]Netherlands Translational Research Center B.V., The Netherlands

Corresponding author: p.h.elsinga@umcg.nl; Tel.:+31-50-361-3247

First author: g.dos.santos.clemente@umcg.nl; Tel.:+31-50-361-3541

Word count: 6384

Short running title: Mapping arginase expression with PET

ABSTRACT

Arginase hydrolyzes L-arginine and influences levels of polyamines and nitric oxide (NO'). Arginase overexpression is associated with inflammations and tumorigenesis. Thus, radiolabeled arginase inhibitors may be suitable positron emission tomography (PET) tracers for staging arginase-related pathophysiologies. We report, for the first time, the synthesis and evaluation of radiolabeled arginase inhibitors, ^{18}F-FMARS and ^{18}F-FBMARS, developed from α-substituted-2-amino-6-boronohexanoic acid derivatives. **Methods:** Arylboronic ester-derived precursors were radiolabeled via copper-mediated fluorodeboronation. Binding assays using arginase-expressing PC3 and LNCaP cells were performed. Autoradiography of lung sections from a guinea pig model of asthma overexpressing arginase, and dynamic micro-PET imaging with PC3-xenografted mice evaluated the radiotracers' specific binding and pharmacokinetics. **Results:** ^{18}F-Fluorinated compounds were obtained with radiochemical yields up to 5% (decay-corrected) and average molar activity of 53 GBq.µmol^{-1}. Cell and lung section experiments indicated specific binding which was blocked up to 75% after pretreatment with arginase inhibitors. Micro-PET studies indicated fast clearance of the radiotracers (7.3±0.6 min), arginase-mediated uptake, and a selective tumor accumulation (standardized uptake value: 3.0±0.7). **Conclusion:** The new ^{18}F-fluorinated arginase inhibitors have the potential to map increased arginase expression related to inflammatory and tumorigenic processes. ^{18}F-FBMARS showed the highest arginase-mediated uptake in PET imaging and a significant difference between the uptake in control and arginase-inhibited PC3 xenografted mice. These results encourage further research to examine the suitability of ^{18}F-FBMARS to select patients for treatments with arginase inhibitors.

Keywords: fluorine-18; arginase; arginase inhibitors; positron emission tomography

INTRODUCTION

Arginase is a manganese-dependent metalloenzyme that catalyzes the hydrolysis of L-arginine to L-ornithine and urea. Cytosolic arginase type I (Arg1) is predominantly expressed in the liver and involved in ureagenesis, whereas mitochondrial type II (Arg2) is expressed throughout extrahepatic tissues (*1*). Arginase levels inversely influence the activity of endothelial, neuronal, and inducible nitric oxide synthases (e/n/iNOS), a group of enzymes competing for the same substrate (L-arginine) to catalyze the production of nitric oxide (NO·). This highly diffusive and reactive gas is important in cell signaling to induce, e.g., relaxation of airway and vascular smooth muscle, neurotransmission, and regulation of the immune system (*2*). The delicate arginase/NOS physiological equilibrium can be disrupted by oxidative and inflammatory signaling pathways (Figure 1) (*2,3*).

Arginase overexpression, and the consequent reduction of NO· and increase of proline and polyamines levels, have been associated with a series of pathologies that range from cardiovascular, immune-mediated, and inflammatory conditions to mental disorders (*2*). Additionally, arginase is upregulated by myeloid cells in several tumor microenvironments at very early stages, being associated with poor outcomes (*4*). Moreover, tumor cells typically overexpress arginase to promote cell proliferation and evade the immune system (*5*). Thus, arginase is a potential therapeutic target, and potent arginase inhibitors were developed (*2,6-8*).

Some of the most potent arginase inhibitors reported in the literature were developed and patented by MARS Inc. (*9,10*). The presence of a chlorophenyl ring in some of these compounds (Figure 2A) encouraged us to synthesize ^{18}F-fluoroanalogs via Cu-mediated late-stage radiofluorination (Figure 2B). Since PET has shown high sensitivity and specificity to measure the expression of certain enzymes (e.g., esterases, glycosylases, hydrolases, proteases (*11*)), we

postulated that arginase imaging could be valuable for the detection and follow-up of arginase-related pathologies. As there are no radiotracers specifically targeting arginase reported in the literature, we developed, for the first time, two ^{18}F-fluorinated quaternary α-amino acid-based arginase inhibitors derived from MARS compounds.

MATERIALS AND METHODS

General Information

All substrates, reagents, and solvents were purchased from commercial suppliers and used as received without any purification unless otherwise noted. Air- and moisture-sensitive manipulations were performed using oven-dried glassware under an atmosphere of argon or nitrogen. Air- and moisture-insensitive reactions were carried out under ambient atmosphere and monitored by thin-layer chromatography on silica gel (TLC-SG) or liquid chromatography-mass spectrometry (LC-MS). Microwave reactions were performed in a Biotage Initiator Classic microwave. Thin-layer chromatography was performed on pre-coated silica gel 60 F$_{254}$ plates and visualized by fluorescence quenching under UV light. Flash chromatography purifications were performed using commercial normal-phase silica gel (40–63 µm particle size). Concentration under reduced pressure was performed by rotary evaporation at 23–40 °C at an appropriate pressure. Final products were purified by Grace Reveleris X2 Column chromatography using Grace Reveleris Silica cartridges (12g or 40g). Purified compounds were further dried under vacuum (10^{-6}–10^{-3} bar). Yields refer to purified and spectroscopically pure compounds.

Aqueous ^{18}F-fluoride used in this work was produced by the ^{18}O(p,n)^{18}F nuclear reaction in an IBA (Louvain-la-Neuve, Belgium) Cyclone 18/9 cyclotron. Manual radiolabeling was

performed in radiochemistry fume hoods at negative air pressure with respect to the laboratory. Radiolabeled products were monitored and identified by radio-TLC and radio-HPLC.

High-resolution mass spectra (HRMS) were obtained using electrospray ionization (ESI) mass spectra (MS) system from Waters Investigator Semi-prep 15 Super Critical Fluid Chromatography (SFC) with a 3100 MS-ESI detector using a solvent system of methanol (with ammonium hydroxide as an additive) and CO_2 on an ethyl pyridine 4.6x250 mm column or from the taken TLC-SG plate using an Advion plate express TLC-MS. Semi-preparative high-performance liquid chromatography (HPLC) was performed on a Waters system using a 1525 binary HPLC pump, a 2489 UV/visible detector and a Berthold Technologies Flowstar LB 513 radio flow detector. Analytical analysis of the synthesized radiotracers for assessment of final quality control (QC) was acquired using a Waters Acquity integrated system coupled to a Berthold Technologies Flowstar LB 513 radio flow detector. HPLC data were processed with Waters Empower 3 software. Radio-TLC's were scanned using a Perkin Elmer Packard Cyclone storage phosphor system and the acquired data analyzed with the OptiQuant 03.00 software. Gamma-counting was performed on a Perkin Elmer Wallac Wizard 1470 (Turku, Finland), with an open energy window (15-1000 keV) and 15 seconds of measuring time.

Nuclear magnetic resonance (NMR) spectra were recorded on a Bruker 500 spectrometer operating at 500 MHz and 126 MHz for ^{1}H and ^{13}C acquisitions, respectively, in deuterated solvents. For ^{1}H NMR, chemical shifts (δ) are reported in ppm, with the solvent residual peak as the internal standard, and coupling constants (J) in hertz (Hz). The following abbreviations were used for spin multiplicity: s = singlet, d = doublet, t = triplet, q = quartet, m = multiplet. Chemical shifts for ^{13}C NMR were reported in ppm relative to the solvent peak.

All animal procedures were carried out following the European Union directives for animal experiments (86/609/CEE, 2003/65/CE, and 2010/63/EU), and the protocols used (AVD105002016395 for mice works, and AVD10500201581 for guinea pig works) were previously approved by the Dutch National Committee on Animal Experiments and the Institutional Animal Care and User Committee of the University of Groningen.

mRNA Isolation and PCR Analysis

Total mRNA was isolated using Trizol RNA extraction (TRI Reagent Solution, Applied Biosystems, Landsmeer, Netherlands), according to the manufacturer's instructions. cDNA was synthesized from equal amounts of RNA using Reverse Transcriptase System (Promega, Madison, WI, USA), and the following protocol: 10 min 25°C, 45 min 42°C, 5 min 99°C. rtPCR was performed with SYBR Green (Roche Diagnostics, Almere, Netherlands) and the following protocol including a final step to generate the melting curve: 2 min 95°C, 10 min 95 °C, 45× (30 s 95°C, 30 s 60°C, 30 s 72°C), 30 s 95°C, 30 s 55°C, 30 s 95°C. The rtPCR was performed in an Eco Illumina (Illumina, Eindhoven, Netherlands). For analysis, the LinReg software was used to calculate N0-values, which were normalized to N0 of *the housekeeping genes* HPRT1 and GAPDH as an internal control. Primer sets used to analyze gene expression are:

Gene:	Forward primer	Reverse primer:
HPRT1	AAGCCAGACTTTGTTGGATT	ACTGGCGATGTCAATAGGAC
GAPDH	CCAGCAAGAGCACAAGAGGA	GAGATTCAGTGTGGTGGGGG
ARG1	GGAGACCACAGTTTGGCAAT	CCACTTGTGGTTGTCAGTGG
ARG2	TGCATCCTTGAACTGTCAGC	ACAAGCTGCTGCTTTCCATT

Surface Plasmon Resonance

Binding kinetics of the inhibitors were determined by surface plasmon resonance using a Biacore T200 (GE Healthcare). Arg1 was immobilized on a Ni-nitrilotriacetic acid sensor chip by Ni-mediated affinity capturing and amine-coupling to a level of 4000 or 6000 resonance units using 60 µg/mL Arg1 in running buffer (50 mM Na_2HPO_4, pH 7.4,150 mM KCl, and 0.01% Tween-20). The arginase inhibitors were diluted in the same running buffer and were injected in an increasing concentration range of 0.1, 0.316, 1.0, 3.16, and 10 µM. Single-cycle kinetics were used for measuring compound binding with a flow rate of 30 µL/min, an association time of 100 s per injection, and a dissociation time of 1800 s. The compound response was subtracted with both the reference channel response and the blank injection. The Biacore Evaluation software was used to fit the data to the Langmuir 1:1 binding model, with x^2 values indicating minimal deviation between the fit and the experimental data. This minimal deviation was confirmed by determination of the reliability of the curve fits with standard Biacore checks. All combinations of the inhibitors and pH conditions were measured in at least two technical replicates to determine the kinetic constants k_a, k_d, and K_D. The target residence time (τ) was calculated from the k_d value using the formula $\tau=1/k_d$.

PET Acquisition, Image Reconstruction, and Biological Half-life Calculation

The anesthetized animals were placed in the micro-PET table in a prone position, on top of a heating pad at 38°C to keep constant body temperature, stretched out as much as possible to minimize organ superposition and with the tumor in the field of view. Subsequently, a 90 minutes emission scan was acquired with a Focus 220 rodent scanner (Siemens/Concorde). Between the injection time and the beginning of the scan, an average time of 5 minutes has passed. After completion of the PET scan, a 10 minutes transmission scan with a [57]Co point source was obtained for the correction of scatter and attenuation of 511 keV photons by tissue.

For the micro-PET image analysis, all emission scans were iteratively reconstructed (OSEM2d, 4 iterations, 16 subsets) after being normalized and corrected for attenuation and radioactive decay. The list-mode data of the emission scans were separated into 24 frames (6x10s, 4x30s, 2x60s, 1x120s, 1x180s, 4x300s, and 6x600s). A three-dimensional volume of interest (VOI) was manually drawn by a single observer on the original data set, delineating the desired area on the summed PET images (0–90 min) using the PMOD software package (version 3.9; PMOD Technologies LLC). These VOIs were used to create the corresponding time-activity curves and to calculate standardized uptake values (SUV). A single exponential curve was fitted to the SUV time-activity curves (using values from 40 to 90 min) by an iterative nonlinear least-squares approach using GraphPad Prism version 6.01 for Windows (GraphPad Software, La Jolla, CA, USA) to calculate the biological half-life of the tracer.

Synthesis and Characterization

Arginase and NOS inhibitors, 2-(*S*)-amino-6-boronohexanoic acid (ABH) and N^{ω}-nitro-L-arginine methyl ester (L-NAME), respectively, were purchased (Merck) with purity ≥98%. The synthesis of the MARS-derived standards (FMARS and FBMARS), and respective arylboronic ester labeling precursors, was performed by modifying a reported method (*10*). These compounds were used as a racemic mixture per the original reports (*9,10*) since the inhibitory potencies and pharmacokinetics of these Cα-substituted ABH derivatives do not significantly differ from the optically active references (*12,13*). Synthesis details, characterization, instrumentation, and additional techniques are given in the Supplemental Data.

Radiolabeling

The Cu-mediated radiofluorination of the arylboronic ester derivatives was performed according to the reported alcohol-enhanced method (*14*) with our previous optimizations (*15,16*).

Aqueous ^{18}F-fluoride (5–10 GBq) was trapped on an anion-exchange cartridge (Chromafix 45-PS-HCO$_3^-$), washed with 1 mL n-butanol, dried with argon, and eluted with 0.4 mL of a tetraethylammonium bicarbonate solution in n-butanol (6.75 mg.mL^{-1}). To this ^{18}F-fluoride solution was added 0.8 mL of dimethylacetamide containing the labeling precursor (4.5 µmol) and [Cu(OTf)$_2$(py)$_4$] (20 µmol). This mixture was stirred at 150°C for 30 minutes. Then, it was diluted in 40 mL of water and passed through an Oasis HLB solid-phase extraction cartridge to trap the ^{18}F-fluorinated intermediate. After washing the cartridge with water (10 mL), the ^{18}F-fluorinated intermediate was recovered with 1.5 mL ethanol, and 0.6 mL HCl 6 N was added to remove the protecting groups. This mixture was left under stirring at 120°C for 30 minutes. The final product, ^{18}F-FMARS or ^{18}F-FBMARS, was isolated by high-performance liquid chromatography (HPLC). A Luna C18 5µm 10x250 mm 100 Å (Phenomenex) column was used with a linear gradient from 100% to 80% aqueous trifluoroacetic acid (TFA, 0.1%) in acetonitrile over 30 minutes (flow of 5 mL.min^{-1}). The collected peak was diluted in water, the solvent was exchanged by trapping the product in an Oasis HLB cartridge and recovered with ethanol. The final solution was diluted with sodium acetate 0.02 M, pH 7.4 (maximum 9% ethanol).

Radiotracer Characterization

The radiotracers' purity was confirmed by: (i) thin-layer chromatography, TLC-Al$_2$O$_3$ developed in n-butanol:CH$_3$COOH:H$_2$O (12:3:5) and; (ii) radio-HPLC using a Gemini-5 µm, C18, 110 Å, LC 150x4.6 mm (Phenomenex) column with linear gradient from 100% to 50% of aqueous 0.1% TFA in acetonitrile over 15 minutes (flow of 1.5 mL.min^{-1}).

The lipophilicity (log D) was measured by dissolving each radiotracer in a 1:1 mixture of phosphate-buffered saline pH 7.4 (PBS) and n-octanol. This mixture was thoroughly vortexed, centrifuged (3000 rpm for 5 min), and left to rest. Triplicate samples from both phases were

measured on a ɣ-counter. The reported log D value is the averaged ratio between the number of counts in the *n*-octanol and PBS layers.

For the in vitro stability assays, each radiotracer was left at room temperature and analyzed by radio-HPLC and radio-TLC at distinct time points up to 4 hours. The stability was also evaluated by incubating the radiotracers with serum at 37°C, analyzed directly by radio-TLC, and after deproteinization with acetonitrile by radio-HPLC, at various time points up to 4 hours.

Enzyme-Substrate Kinetics

ABH, MARS, FMARS, and FBMARS were evaluated for their ability to inhibit recombinant human arginase 1 and 2. Half-maximal inhibitory concentration (IC_{50}) values were obtained with a colorimetric urea inhibition assay (*8,12*) performed in 96-wells plates with a final volume of 60 μL per well for each reaction. Each arginase subtype (0.67 μg/mL) was pre-incubated with five concentrations (0.0167-167 μM) of the arginase inhibitors in PBS, for 30 minutes at 37˚C. The reactions started by adding 10 μL of L-arginine (120 mM) and left to incubate for 1h at 37˚C. After quenching, the arginase activity was quantified with a Synergy H1 Microplate Reader (Biotek) by spectrophotometric measurement (530 nm) of the urea produced, and the IC_{50} values were calculated.

The enzyme-substrate binding kinetics of the arginase inhibitors were monitored in real-time with a non-invasive label-free surface plasmon resonance ResidenceTimer™ assay developed by the Netherlands Translational Research Center (Oss, The Netherlands) in a BiaCore T200 (GE Healthcare) system (*17*). As no differences were seen between the IC_{50} values for Arg1 and Arg2, and no significant changes in binding kinetics between isoforms are expected, only Arg1 was used for the kinetic assays. Arg1 was diluted in 50 mM Na_2HPO_4, pH 7.4, 150 mM KCl, and 0.01% Tween-20, in a concentration of 60 μg/mL, and immobilized on a sensor chip.

Five concentrations (0.1-10 µM) of the arginase inhibitors were injected into the system to measure binding.

Cell-Binding Assays

Mycoplasma-free arginase-expressing LNCaP and PC3 cell lines ([18-22]) obtained from the American Type Culture Collection (cultured in RPMI-1640 medium with 10% fetal bovine serum) were washed with PBS (37°C) and left for 30 minutes in PBS enriched with glucose (5.6 mM), $MgCl_2$ (0.49 mM), and $CaCl_2$ (0.68 mM) (PBS-GMC), at 37°C (5% CO_2). For control assays, 25 µL of PBS was added to the wells. For competition assays, 25 µL of ABH, MARS, FMARS, or FBMARS in PBS (1 mM/well) was added. For the arginase/NOS specificity assays, 25 µL of L-NAME (1 mM/well), or 12.5 µL of L-NAME (1 mM/well) with 12.5 µL of MARS (1 mM/well) was added. After 30 minutes of pre-incubation (5% CO_2, 37°C), 50 µL of the radiotracer (4 MBq.mL^{-1}) was added to each well and left to incubate for another 30 minutes. Finally, the medium from all wells was removed and the cells were washed with cold PBS, trypsinized, detached, resuspended in medium (RPMI-1640 10% fetal bovine serum, 37ºC), and transferred to test tubes. Each tube's radioactivity was determined in a ɣ-counter, and the viable cells counted after trypan blue treatment.

Autoradiography Assays

A well-defined guinea pig model of asthma, showing increased expression of arginase in the lungs, has been developed by Meurs and co-workers ([23-25]). 8 male Dunkin Hartley guinea pigs (Envigo, Netherlands) weighing approximately 250 grams at the time of sensitization were used. The guinea pigs were housed conventionally in pairs, in ventilated cages in rooms maintained at a 12 hour light/dark cycle, and were provided *ad libitum* access to food and water. The radiotracers were evaluated in 4 µm pulmonary cross-sections of this model. The lung

sections of ovalbumin-sensitized guinea pigs challenged with saline (healthy control) or allergenic ovalbumin (asthmatic model) were washed by soaking in a solution of Trizma® HCl (pH 7.4, 0.05 M) with NaCl (120 mM), $CaCl_2$ (2 mM), and $MgCl_2$ (5 mM), left in this medium for 30 minutes and then gently dried with an air stream. Each lung section was covered with 300 µL of a mixture of radiotracer (0.4 MBq) with/without an arginase inhibitor (1 mM) and left to incubate for 60 minutes. After incubation, all lung sections were washed with cold Trizma® HCl (pH 7.4, 0.05 M), ice-cold water, and dried. These sections were then exposed to a phosphor imaging screen and quantified by a GE Healthcare Amersham Typhoon autoradiograph.

Animal Studies

Immune deficient mice were inoculated with PC3 cells, which have higher tumorigenicity than LNCaP (*26*). 32 immunocompromised male mice (6-8 weeks old BALB/c nude mice supplied by Envigo, Netherlands) were used. The animals were provided with sterilized chow and water *ad libitum*, and housed in individually ventilated cages equipped with a negative-pressure HEPA filtered air system. During tumor inoculation or PET scanning, the mice were anesthetized with isoflurane (5% for induction and 2% for maintenance). Arginase gene expression in the PC3 cells was confirmed by real-time polymerase chain reaction (Supplemental Figure 1). Inoculations were performed subcutaneously on each mouse's neck with a suspension of 2.0 ± 1.0 x 10^6 PC3 cells in a 1:1 mixture of Matrigel® and RPMI-1640 medium with 10% fetal bovine serum. Mice were scanned when tumors reached 0.45 ± 0.15 cm^3. Tumor diameters were measured 1 to 3 times per week with a caliper, and tumor volume was calculated using the following formula: $V_{tumor} = ab^2/2$, where a and b represent tumor length and width, respectively). The body mass of all animals at the time of the radiotracer injection was 21.3 ± 0.3 g. The radiotracer (4.2 ± 1.5 MBq; 92 ± 56 pM of molar mass estimated from the injected dose and molar

activity) was administered through the penile vein with/without co-injection of arginase inhibitor (5 mM). After a dynamic 90-minute emission scan and a 10-minute transmission scan on a Focus 220 tomograph (Siemens/Concorde), animals were euthanized, and urine and blood were collected to assess the radiotracer stability. Organs and tumors were harvested, weighed, and the radioactivity was determined to calculate the percentage of injected dose per gram of tissue (%ID/g). For the micro-PET image analysis, three-dimensional volumes of interest delineating the desired area on the summed PET images (0–90 min) were drawn using PMOD software (version 3.9; PMOD Technologies LLC). For in vivo stability, urine and blood samples were collected approximately 2 hours after injecting the radiotracer in BALB/c nude mice. Urine was directly analyzed by radio-HPLC and radio-TLC. Aliquots of the blood samples were directly analyzed by radio-TLC. The remaining blood was centrifuged (6000 rpm for 3 min) to separate the plasma fraction. Plasma was directly analyzed by radio-TLC and, after deproteinization with acetonitrile, by radio-HPLC.

Statistics

Data are expressed as the mean±standard deviation. All experiments were repeated at least three times independently. Unpaired two-tailed t-tests were used for statistical evaluations. A $P<0.05$ was considered statistically significant. Statistical analyses were performed using GraphPad Prism v6.01.

RESULTS

Compound Characterization and Radiolabeling

The synthesis of MARS, FMARS, and FBMARS yielded 16±3% for all three compounds. Further evaluation of these arginase inhibitors confirmed their similar potency to inhibit both enzyme isoforms indistinctly (IC$_{50}$: 0.04-1.4 µM, Table 1). The binding affinities (K_D) of all arginase inhibitors to Arg1 were similar (148-438 nM) and in agreement with the literature (*27*). Results are shown in Table 1 and Supplemental Figure 2.

^{18}F-FMARS and ^{18}F-FBMARS were radiosynthesized from the respective arylboronic ester precursors, purified, and reformulated into injectable solutions in approximately 105 minutes. A final radiochemical yield of 4±1% (decay-corrected) was achieved with a molar activity of 53±19 GBq.µmol^{-1}. Both radiotracers showed a radiochemical purity >95%, either at the end of synthesis (Supplemental Figure 3) or during the stability studies in solution or serum up to 4 hours (Supplemental Figures 4-7). A log D of -0.7±0.1 and -1.0±0.1 (at pH 7.4) was experimentally calculated for ^{18}F-FMARS and ^{18}F-FBMARS, respectively.

Cell-Binding Assays

Both radiotracers showed cellular uptake associated with arginase expression, as this binding effect was reduced after pretreatment with competitive inhibitors (Figure 3). The overall blocking efficiency in both cell lines was 47±8% for MARS, FMARS, and FBMARS, while for ABH it was 22±6%. Cells were also pre-treated with the selective NOS inhibitor L-NAME to confirm specificity for arginase. When PC3 cells were incubated with L-NAME and an arginase inhibitor, the tracer's uptake decreased 50±5% (*P*=0.0002).

Asthmatic Lung Model

Incubation of ^{18}F-FMARS and ^{18}F-FBMARS with control lung sections showed residual binding, while an approximately 10-fold increase was seen in sections from allergen-challenged

animals (Figure 4, Supplemental Figure 8), correlating to the well-characterized overexpression of arginase in this asthmatic model (*24,25*). The blocking effect in asthmatic lung sections treated with arginase inhibitors (max. 60%, *P*=0.02) reiterated radiotracers' specificity towards arginase.

^{18}F-FMARS/^{18}F-FBMARS Biodistribution

After confirmation of arginase gene expression in the PC3 cells, immunocompromised mice were inoculated with this cell line (Supplemental Figure 9). A pilot screening was performed with ^{18}F-FBMARS in the PC3 xenograft model to evaluate which arginase inhibitor (ABH or MARS) shows superior in vivo inhibitory effect. By significantly reducing tumor uptake (Supplemental Figure 10), ABH was selected to evaluate the in vivo arginase specificity of both radiotracers.

Biodistribution studies with ^{18}F-FMARS and ^{18}F-FBMARS after micro-PET scans, confirmed arginase-mediated uptake (Figure 5, Supplemental Table 1). A generalized decline of the uptake in ABH co-injection experiments was also seen due to arginase ubiquity (*28*). Relatively high uptake in the kidneys and moderate uptake in the liver indicates a preference for urinary excretion but can also be related to high expression of arginase in these organs, since uptake was reduced by ABH. A prominent blocking effect in endocrine and intestinal tissues was observed, as these are known to highly express Arg2 (*29*). The %ID/g for harvested tumors showed a significant reduction of ^{18}F-FBMARS uptake (70±19%, *P*<0.0001) after ABH co-injection. Combined with a tumor-to-organ ratio generally higher than two (Supplemental Figure 11), this highlights the particular potential of ^{18}F-FBMARS to differentiate arginase overexpressing tumors from non-target tissues. Radiometabolites and ^{18}F-defluorination products were not detected in plasma and urine analysis (Supplemental Figures 12-15).

Micro-PET Imaging

A 90-minute dynamic PET study was performed in mice bearing PC3 tumors to evaluate the potential of ^{18}F-FMARS and ^{18}F-FBMARS to map arginase expression in vivo (Figure 6). A maximum standardized uptake value of 3.1±0.7 in the tumor and a signal reduction up to 60% ($P<0.01$) when ABH was co-injected confirmed an arginase-mediated uptake. Furthermore, due to the generalized arginase expression, a decrease in tracer's uptake was seen after treatment with arginase inhibitor, especially in the salivary and Harderian glands known to highly express arginase (*30*).

Time-activity curves indicated rapid blood clearance for both radiotracers (Figure 7), as maximum uptake in the heart was reached in less than 5 minutes post-injection, decreasing then exponentially with a biological half-life of 7.3±0.6 minutes. Accumulation of ^{18}F-FMARS and ^{18}F-FBMARS in PC3 tumors was clearly visualized, reaching a peak at approximately 40 minutes post-injection with a subsequent slow decrease (biological half-life approx. 105 minutes). When the radiotracers were co-injected with ABH, the accumulation in the PC3 tumors was lower, reaching its maximum 17.5 minutes after injection, and then decreasing exponentially more rapidly than in controls (biological half-life of 67.7±8.1 minutes). However, the difference in tumor uptake between control and ABH treated groups only became statistically significant approximately 33 minutes after the ^{18}F-FBMARS injection.

DISCUSSION

The substitution of a chlorophenyl (MARS) by a fluorophenyl group (FMARS) did not affect the affinity or inhibitory potency to arginase but reduced the residence time on the active site. The longer residence time of MARS indicates a better potential to treat arginase-overexpressing pathologies due to prolonged pharmacodynamic effect. Nevertheless, reversible

inhibitors such as Cα-substituted ABH derivatives (*7*) have a high association rate constant (k_a), favouring PET imaging. Their radiolabeled analogs will rapidly accumulate in sites with high expression of the target enzyme and more effectively clear from non-target regions (*11*). The rapid clearance of these arginase inhibitors (*31*) may result in less background signal.

To increase k_a, the piperidine moiety of FMARS was replaced by a tropane group (FBMARS) (*10*). This modification locks the molecule in a conformation that benefits interaction with the amino acid residues of the active site (*10*), leading to a 10-fold increase in arginase inhibitory activity and enzyme-inhibitor complex formation rate. Thus, to evaluate arginase mapping potential, ^{18}F-fluorinated analogs (^{18}F-FMARS and ^{18}F-FBMARS) were successfully synthesized with molar activity comparable to other ^{18}F-labeled tracers used in the clinic (*32*).

Preliminary assays in arginase-overexpressing prostate cancer cells showed specific binding of both radiotracers to arginase, as the cellular uptake decreased after pretreatment with arginase inhibitors. The specificity of the radiotracers to arginase over NOS was confirmed by the inefficiency of the selective NOS inhibitor L-NAME to affect ^{18}F-FMARS and ^{18}F-FBMARS uptake. Non-specific residual binding was visible after pretreatment with arginase inhibitors, which was expected since boronic acids are known to react with carbohydrates in the cell membrane (*33*). This interaction is common to all classical boronic acid inhibitors at physiological pH.

Competitive binding assays with results comparable to those obtained in cells were seen in guinea pigs' lung sections. A 10-fold increase in the binding of both radiotracers to allergen-challenged lungs was seen, which is related to the overexpression of arginase in the asthmatic airways (*24,25,34*). ^{18}F-FMARS and ^{18}F-FBMARS uptake was reduced after pretreatment of the asthmatic lung sections with arginase inhibitors. An increased arginase expression is also present

in the lungs of asthmatic patients and associated with higher severity (*35,36*). Arginase inhibitors are therefore considered as a potential therapeutic approach to treat asthma (*6*). FBMARS may be considered as a candidate drug, while ^{18}F-FMARS or ^{18}F-FBMARS may become imaging tools for patient selection or treatment follow-up.

Despite showing weaker inhibition in vitro, ABH demonstrated a more efficient blocking effect than MARS in vivo. Since ABH has K_D, IC_{50}, and hydrophilicity similar to the MARS compounds (*10*), its lower in vitro effect may be explained by a much shorter target residence time (τ). In vitro binding assays involve the abrupt wash out of the unbound substrate, a procedure known to underestimate the efficiency of reversible ligands with brief target residence times when compared to the in vivo assessments (*37*). This discrepancy in the blocking efficiency may also be explained by differences in bioavailability, membrane penetration capacity, or clearance rates between ABH and MARS, or by potential alterations in the expression of cationic amino acid transporters or other endogenous processes between the in vitro and in vivo models used. These observations suggest that novel arginase inhibitors should be evaluated in complex biological systems after being screened with purified arginase or in controlled cellular microenvironments (*12,31*). Thus, real-time assessment of the pharmacokinetics and therapeutic efficacy of arginase inhibitors within living subjects may be facilitated using PET.

The potential of ^{18}F-FMARS and ^{18}F-FBMARS to map arginase expression was evaluated in PC3 xenograft mice. ^{18}F-FBMARS revealed higher tumor-to-organ ratios and more significant uptake differences between control and blocked animals than ^{18}F-FMARS. In vivo assays reaffirmed the radiotracers' specificity since the uptake in the arginase-expressing tumors was clearly reduced with ABH co-injection. Global suppression of radiotracer uptake by ABH was also noticed due to arginase's widespread ubiquity (*28*). ^{18}F-FBMARS produced a more intense

signal than ^{18}F-FMARS, as was also seen in pulmonary autoradiography. The statistically significant difference between ^{18}F-FBMARS tumor uptake with and without inhibitor after 40 minutes of injection makes this radiotracer the best choice for arginase mapping.

Nevertheless, none of the radiotracers showed isozyme selectivity, and molecules with such capacity remain challenging to attain due to the active sites' structural similarity (*38*). Poor selectivity for Arg2 causes undesirable radiotracer uptake in the liver with consequences for dosimetry. Hepatic radiation dose may be reduced by previously administering N^{ω}-hydroxy-L-arginine, known to be up to 18 times more potent in inhibiting arginase activity in the liver than in non-hepatic tissues (*39*).

As the development of therapeutically potent arginase inhibitors is a very active topic, ^{18}F-FBMARS may serve as a potential PET tracer to aid pharmaceutical industry, e.g., by enabling real-time in vivo arginase mapping studies to prove target occupancy and pharmacodynamics of novel molecules. A possible limitation of our tracers may be the poor discrimination between inflammatory and carcinogenic tissues, leading to false positives. However, they may be relevant for immune therapy, as arginase is involved in the regulation of tumor-induced immune tolerance, and arginase inhibition promotes the formation of an inflammatory microenvironment favoring cancer-specific immune response (*40*). Therefore the use of arginase inhibitors has been proposed for the treatment of certain tumors. ^{18}F-FBMARS may be used to select patients who could benefit the most from immunotherapy treatments.

CONCLUSION

We report, for the first time, the development of radiolabeled arginase inhibitors for PET imaging of arginase expression. These ^{18}F-fluorinated arginase inhibitors showed a high affinity towards arginase. ^{18}F-FBMARS showed the highest arginase-mediated uptake in PC3 xenografts. These results encourage further exploration of the suitability of ^{18}F-FBMARS to select patients who can benefit from treatments with arginase inhibitors.

DISCLOSURE

ACKNOWLEDGMENTS

KEY POINTS

Question

Are arginase inhibitors suitable PET tracers for mapping arginase expression?

Pertinent findings

The synthesis and evaluation of radiolabeled arginase inhibitors are reported for the first time. The novel ^{18}F-fluorinated arginase inhibitors showed high affinity and arginase-specific in vivo binding, thus the potential to map increased arginase expression related to inflammatory and tumorigenic processes.

Implications for patient care

Radiofluorinated arginase inhibitors may be explored as PET tracers to select patients who can benefit from treatments with arginase inhibitors.

REFERENCES

1. Dzik JM. Evolutionary roots of arginase expression and regulation. *Front Immunol.* 2014;5:544.

2. Caldwell RW, Rodriguez PC, Toque HA, et al. Arginase: a multifaceted enzyme important in health and disease. *Physiol Rev.* 2018;98:641-665.

3. Moretto J, Girard C, Demougeot C. The role of arginase in aging: a systematic review. *Exp Gerontol.* 2019;116:54-73.

4. Pham T-N, Liagre B, Girard-Thernier C, et al. Research of novel anticancer agents targeting arginase inhibition. *Drug Discov Today.* 2018;23:871-878.

5. Clemente GS, van Waarde A, Antunes IF, et al. Arginase as a potential biomarker of disease progression: a molecular imaging perspective. *Int J Mol Sci.* 2020;21:5291.

6. Meurs H, Zaagsma J, Maarsingh H, van Duin M. Recent patents in allergy/immunology: use of arginase inhibitors in the treatment of asthma and allergic rhinitis. *Allergy.* 2019;74:1206-1208.

7. Pudlo M, Demougeot C, Girard-Thernier C. Arginase inhibitors: a rational approach over one century. *Med Res Rev.* 2017;37:475-513.

8. Van den Berg MPM, Kurhade SH, Maarsingh H, et al. Pharmacological screening identifies SHK242 and SHK277 as novel arginase inhibitors with efficacy against allergen-induced airway narrowing in vitro and in vivo. *J Pharmacol Exp Ther.* 2020;374:62-73.

9. Van Zandt M, Golebiowski A, Ji Min KOO, et al. Inhibitors of arginase and their therapeutic applications. US patent WO 2011/133653 A1. 2011/04/20, 2011.

10. Golebiowski A, Whitehouse D, Beckett RP, et al. Synthesis of quaternary α-amino acid-based arginase inhibitors via the Ugi reaction. *Bioorg Med Chem Lett.* 2013;23:4837-4841.

11. Rempel BP, Price EW, Phenix CP. Molecular imaging of hydrolytic enzymes using PET and SPECT. *Mol Imaging.* 2017;16:1536012117717852.

12. Golebiowski A, Beckett RP, Van Zandt M, et al. 2-Substituted-2-amino-6-boronohexanoic acids as arginase inhibitors. *Bioorg Med Chem Lett.* 2013;23:2027-2030.

13. Blaszczyk R, Brzezinska J, Dymek B, et al. Discovery and pharmacokinetics of sulfamides and guanidines as potent human arginase 1 inhibitors. *ACS Med Chem Lett.* 2020;11:433-438.

14. Zischler J, Kolks N, Modemann D, et al. Alcohol-enhanced Cu-mediated radiofluorination. *Chem Eur J.* 2017;23:3251-3256.

15. Zarganes-Tzitzikas T, Clemente GS, Elsinga PH, Dömling A. MCR scaffolds get hotter with ^{18}F-labeling. *Molecules.* 2019;24:1327.

16. Clemente GS, Zarganes-Tzitzikas T, Dömling A, Elsinga PH. Late-stage copper-catalyzed radiofluorination of an arylboronic ester derivative of atorvastatin. *Molecules.* 2019;24:4210.

17. Grobben Y, Uitdehaag JCM, Willemsen-Seegers N, et al. Structural insights into human arginase-1 pH dependence and its inhibition by the small molecule inhibitor CB-1158. *J Struct Biol.* 2020;4:100014.

18. Cederbaum SD, Yu H, Grody WW, et al. Arginases I and II: do their functions overlap? *Mol Genet Metab.* 2004;81:S38-S44.

19. Sigala S, Bodei S, Missale C, et al. Gene expression profile of prostate cancer cell lines: effect of nerve growth factor treatment. *Mol Cell Endocrinol.* 2008;284:11-20.

20. Mumenthaler SM, Yu H, Tze S, et al. Expression of arginase II in prostate cancer. *Int J Oncol.* 2008;32:357-365.

21. Hsueh EC, Knebel SM, Lo W-H, et al. Deprivation of arginine by recombinant human arginase in prostate cancer cells. *J Hematol Oncol.* 2012;5:17.

22. Ino Y, Yamazaki-Itoh R, Oguro S, et al. Arginase II expressed in cancer-associated fibroblasts indicates tissue hypoxia and predicts poor outcome in patients with pancreatic cancer. *PloS One.* 2013;8:e55146.

23.   Meurs H, Santing RE, Remie R, et al. A guinea pig model of acute and chronic asthma using permanently instrumented and unrestrained animals. *Nat Protoc.* 2006;1:840-847.

24.   Maarsingh H, Zaagsma J, Meurs H. Arginase: a key enzyme in the pathophysiology of allergic asthma opening novel therapeutic perspectives. *Br J Pharmacol.* 2009;158:652-664.

25.   Maarsingh H, Dekkers BGJ, Zuidhof AB, et al. Increased arginase activity contributes to airway remodelling in chronic allergic asthma. *Eur Respir J.* 2011;38:318-328.

26.   Wu X, Gong S, Roy-Burman P, et al. Current mouse and cell models in prostate cancer research. *Endocr Relat Cancer.* 2013;20:R155-R170.

27.   Costanzo LD, Ilies M, Thorn KJ, Christianson DW. Inhibition of human arginase I by substrate and product analogues. *Arch Biochem Biophys.* 2010;496:101-108.

28.   Morris SM, Bhamidipati D, Kepka-Lenhart D. Human type II arginase: sequence analysis and tissue-specific expression. *Gene.* 1997;193:157-161.

29.   Human Protein Atlas available from http://www.proteinatlas.org. Accessed April 5th, 2020.

30.   Yasuda N, Moriwaki K, Furuyama S. Distribution and properties of arginase in the salivary glands of four species of laboratory mammals. *J Comp Physiol B.* 2004;174:237-242.

31.   Abdelkawy KS, Lack K, Elbarbry F. Pharmacokinetics and pharmacodynamics of promising arginase inhibitors. *Eur J Drug Metab Pharmacokinet.* 2017;42:355-370.

32.   Huisman M, Niemeijer A-L, Windhorst B, et al. Quantification of PD-L1 expression with ^{18}F-BMS-986192 PET/CT in patients with advanced stage non-small-cell lung cancer. *J Nucl Med.* 2020;61:1455-1460.

33.   Achilli C, Ciana A, Fagnoni M, et al. Susceptibility to hydrolysis of phenylboronic pinacol esters at physiological pH. *Cent Eur J Chem.* 2013;11:137-139.

34.   Pera T, Zuidhof AB, Smit M, et al. Arginase inhibition prevents inflammation and remodeling in a guinea pig model of chronic obstructive pulmonary disease. *J Pharmacol Exp Ther.* 2014;349:229-238.

35.   Lara A, Khatri SB, Wang Z, et al. Alterations of the arginine metabolome in asthma. *Am J Respir Crit Care Med.* 2008;178:673-681.

36.   Xu W, Comhair SAA, Janocha AJ, et al. Arginine metabolic endotypes related to asthma severity. *PloS One.* 2017;12:e0183066.

37.   Vauquelin G. Rebinding: or why drugs may act longer in vivo than expected from their in vitro target residence time. *Expert Opin Drug Discov.* 2010;5:927-941.

38.   Ash DE. Structure and function of arginases. *J Nutr.* 2004;134:2760S-2764S.

39.   Baggio R, Emig FA, Christianson DW, et al. Biochemical and functional profile of a newly developed potent and isozyme-selective arginase inhibitor. *J Pharmacol Exp Ther.* 1999;290:1409-1416.

40.   Timosenko E, Hadjinicolaou AV, Cerundolo V. Modulation of cancer-specific immune responses by amino acid degrading enzymes. *Immunotherapy.* 2017;9:83-97.
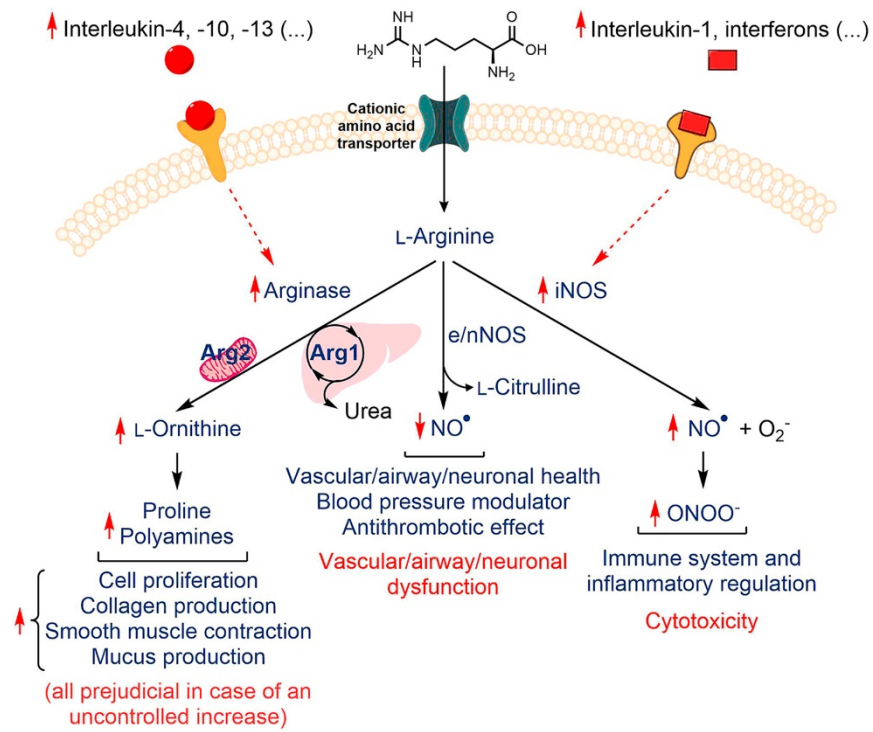
FIGURE 1. L-Arginine metabolism outcomes associated with physiological (blue) and pathophysiological (red) expression of arginase and NOS.
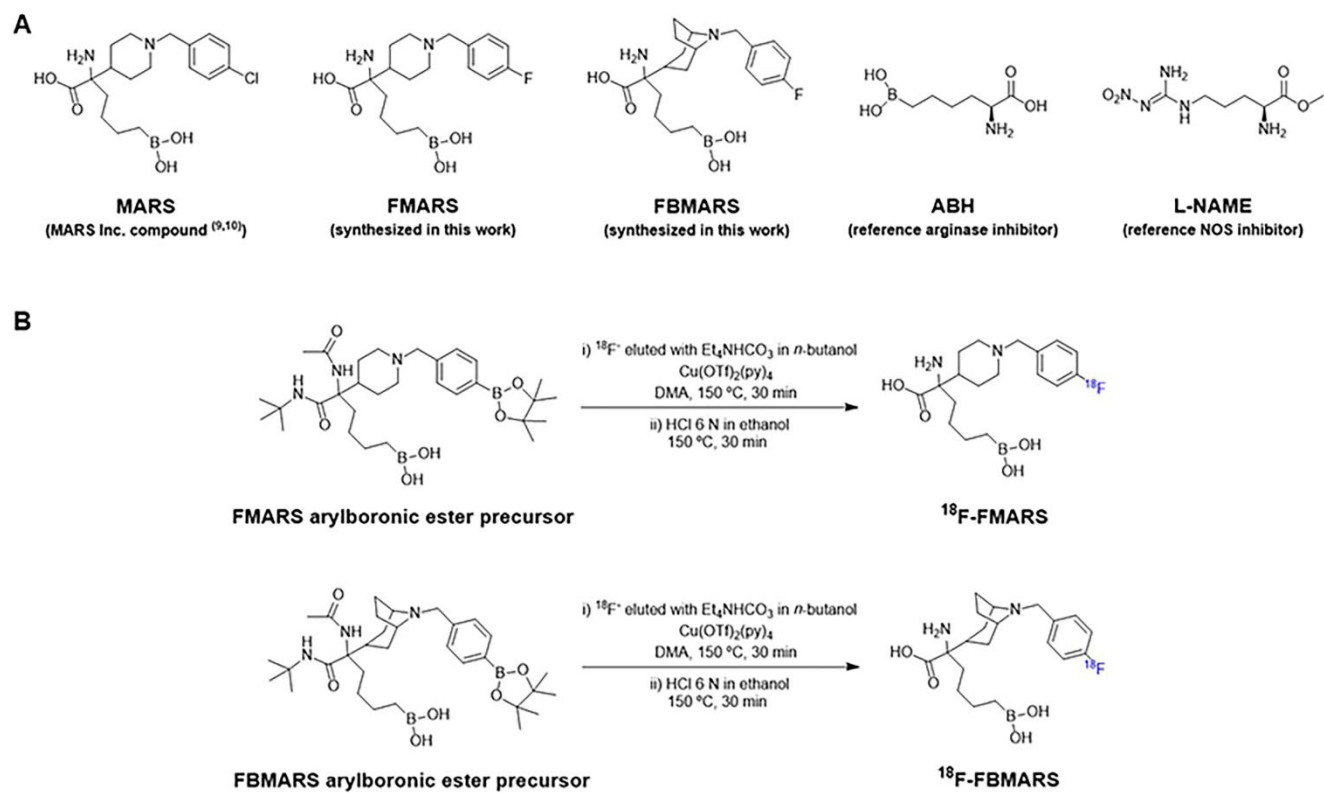
FIGURE 2. Molecules used in this work (A) and arylboronic ester-derived precursors with respective ^{18}F-fluorinated products (B).
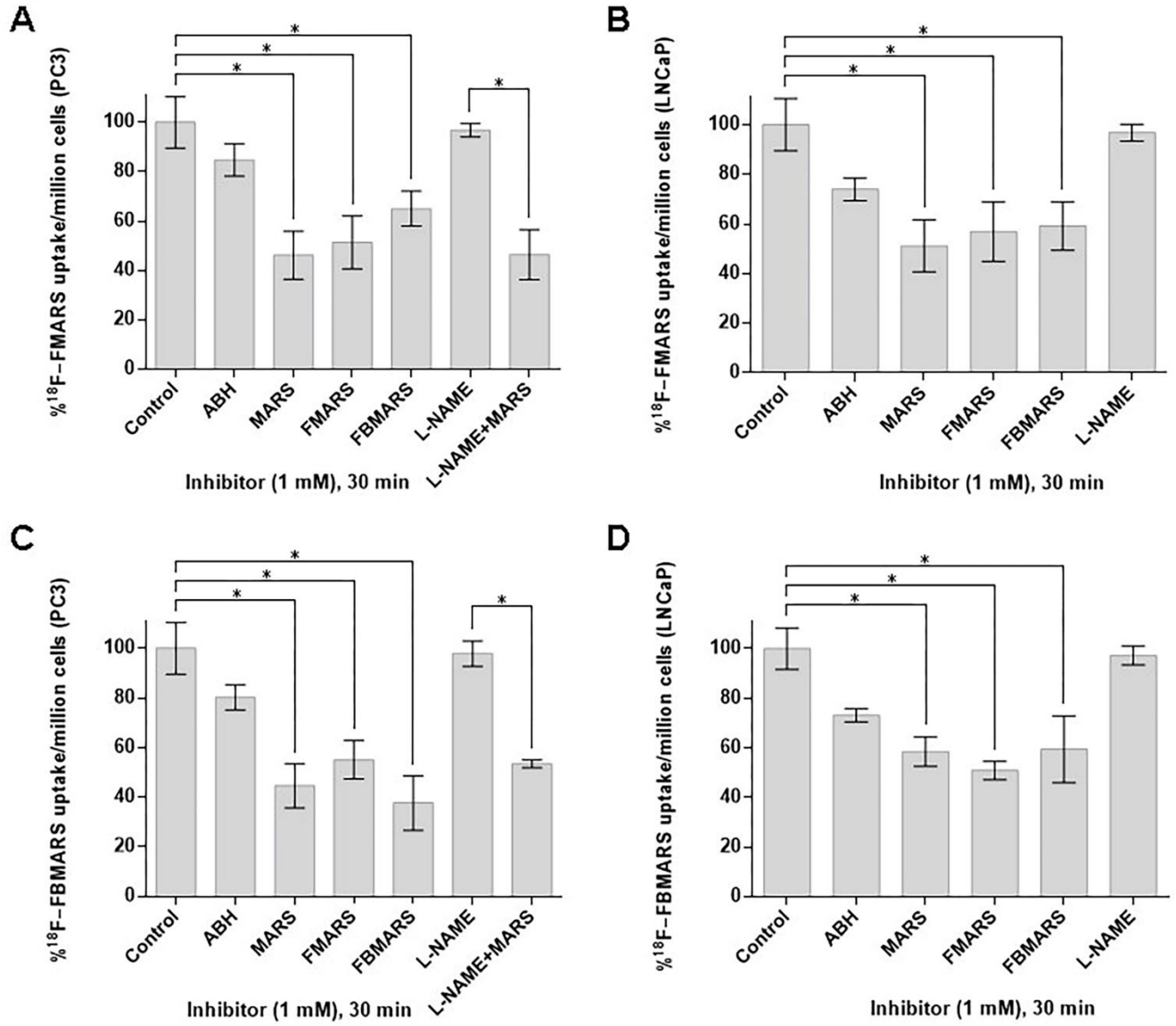
FIGURE 3 ^{18}F-FMARS (A,B) and ^{18}F-FBMARS (C,D) uptake in PC3 and LNCaP cells without (control) and with competitive inhibition ($n \geq 3$, *$P<0.05$). Data expressed as the percentage of cell-associated radioactivity per 1 million cells.
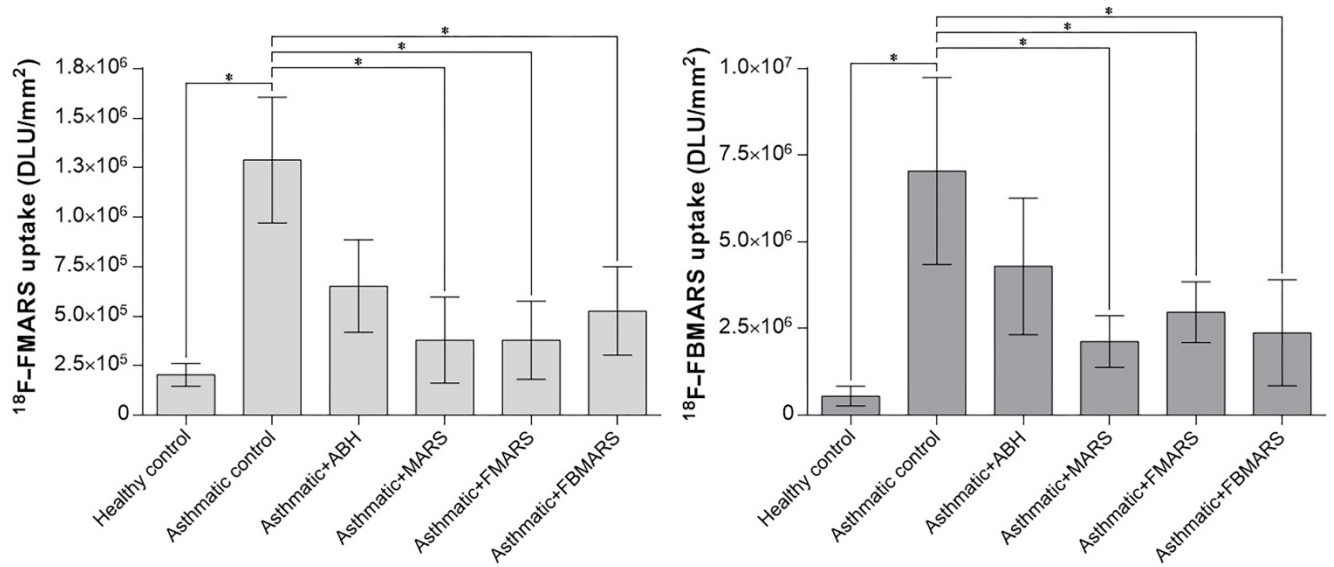
FIGURE 4. ^{18}F-FMARS and ^{18}F-FBMARS uptake in digital luminescence units (DLU) per mm^2 in saline- (healthy) and allergen-challenged (asthmatic) guinea pig lung sections without (control) and with competitive arginase inhibition (n=4, *P<0.05).
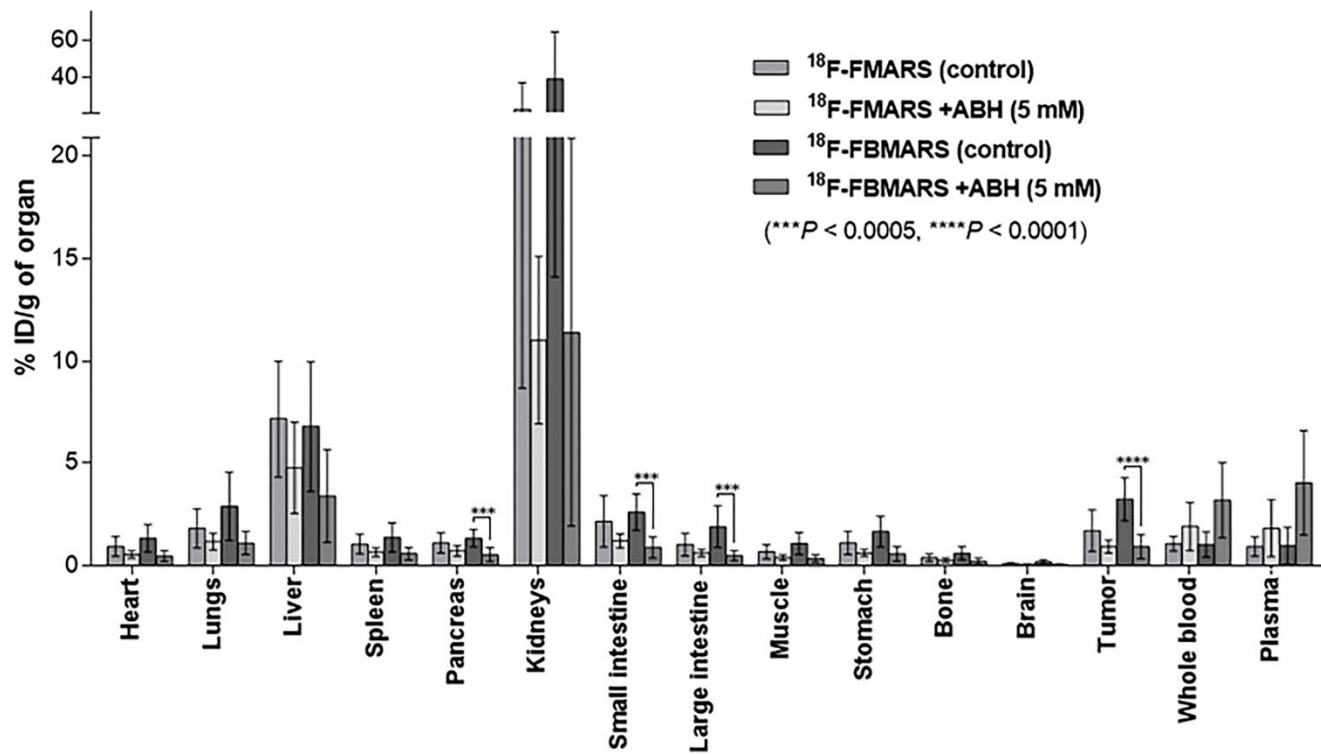
FIGURE 5. Biodistribution of ^{18}F-FMARS (n=7) and ^{18}F-FBMARS (n=9), with and without ABH co-injection, approximately 2 hours after injection in PC3 xenograft mice.
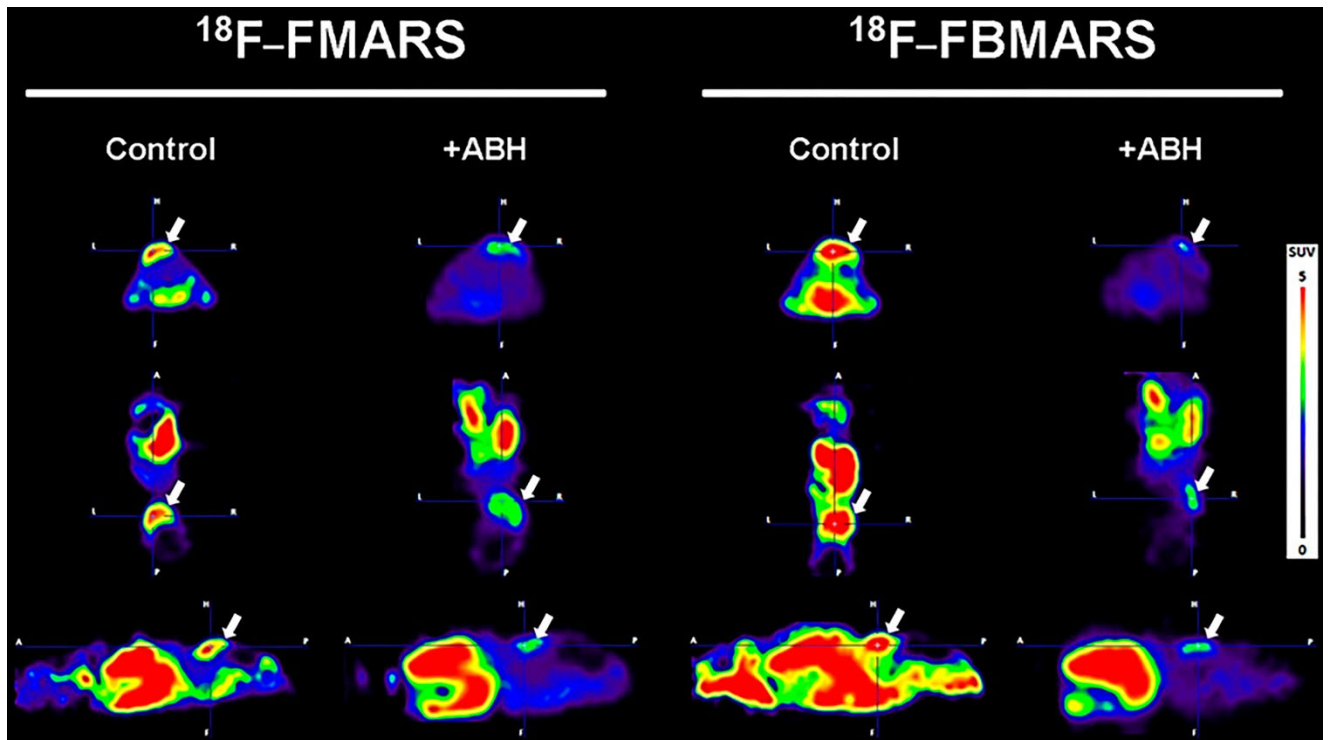
FIGURE 6. Representative maximum intensity micro-PET images (40-90 min) centered at the PC3 tumor (axial, coronal, and sagittal views from top to bottom) of mice injected with ^{18}F-FMARS or ^{18}F-FBMARS, without (control) and with co-injection of ABH (5 mM).
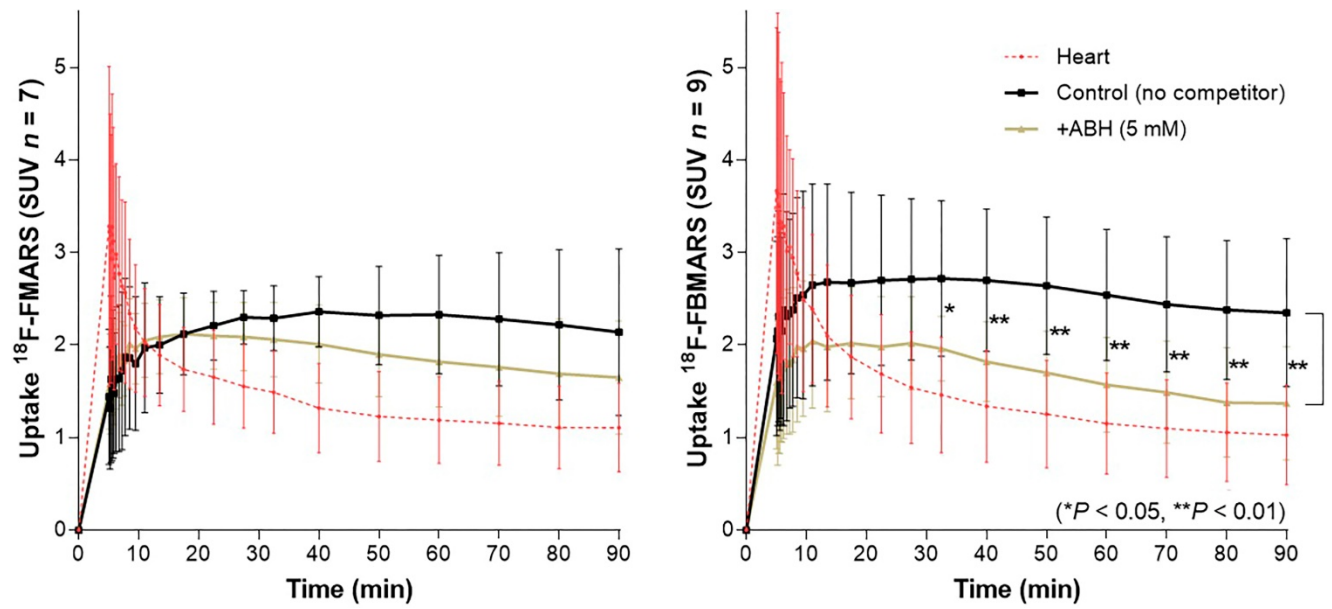
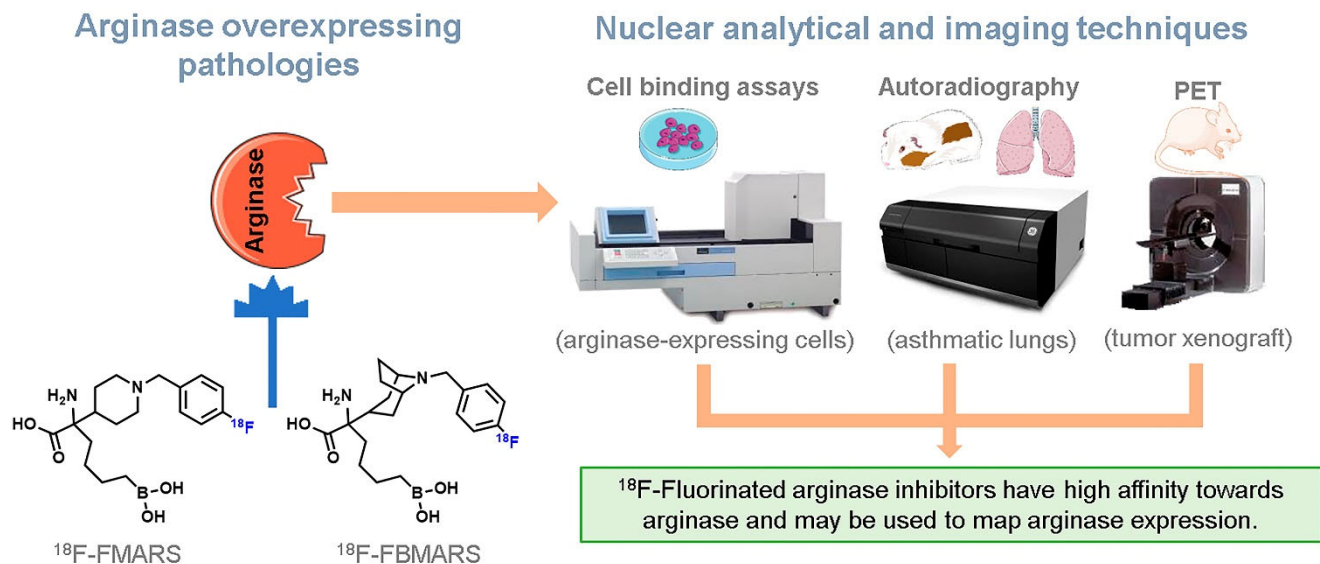**FIGURE 7.** Time-activity curves of ^{18}F-FMARS (n=7) and ^{18}F-FBMARS (n=9). Standardized uptake values (SUV) in PC3 xenograft mice without (control) and with ABH co-injection.

TABLE 1

IC$_{50}$ and enzyme-substrate kinetics of the arginase inhibitors.

| Substrate | IC$_{50}$ (pH 7.4) | | Arg1-substrate kinetics (pH 7.4) | | | | |
	Arg1 (μM)	Arg2 (μM)	$K_D{}^*$ (M)	$k_d{}^\dagger$ (s^{-1})	$k_a{}^\ddagger$ (M$^{-1} \cdot$s^{-1})	t$_{1/2}{}^\S$ (s)	$\tau^\|$ (s)
ABH	1.4	1.1	4.38×10^{-7}	1.10×10^{-2}	2.51×10^4	63	91
MARS	0.9	0.7	1.48×10^{-7}	3.90×10^{-4}	2.64×10^3	1775	2561
FMARS	1.1	0.4	3.16×10^{-7}	8.90×10^{-4}	2.82×10^3	779	1123
FBMARS	0.04	0.05	2.28×10^{-7}	3.47×10^{-3}	1.52×10^4	200	288

$^*K_D$: equilibrium dissociation constant, $K_D = k_d/k_a$. $^\dagger k_d$: dissociation rate constant (fraction of arginase-substrate complexes dissociating per second). $^\ddagger k_a$: association rate constant (arginase-substrate complexes formed per second in 1 M solution). §t$_{1/2}$: dissociative half-life, t$_{1/2}$=ln(2)·τ. $^\|$τ: target residence time, τ=1/k_d.

GRAPHICAL ABSTRACT

Arginase overexpressing pathologies

Nuclear analytical and imaging techniques

Cell binding assays

(arginase-expressing cells)

Autoradiography

(asthmatic lungs)

PET

(tumor xenograft)

^{18}F-FMARS

^{18}F-FBMARS

^{18}F-Fluorinated arginase inhibitors have high affinity towards arginase and may be used to map arginase expression.

SUPPLEMENTARY DATA

General Information

All substrates, reagents, and solvents were purchased from commercial suppliers and used as received without any purification unless otherwise noted. Air- and moisture-sensitive manipulations were performed using oven-dried glassware under an atmosphere of argon or nitrogen. Air- and moisture-insensitive reactions were carried out under ambient atmosphere and monitored by thin-layer chromatography on silica gel (TLC-SG) or liquid chromatography-mass spectrometry (LC-MS). Microwave reactions were performed in a Biotage Initiator Classic microwave. Thin-layer chromatography was performed on pre-coated silica gel 60 F_{254} plates and visualized by fluorescence quenching under UV light. Flash chromatography purifications were performed using commercial normal-phase silica gel (40–63 µm particle size). Concentration under reduced pressure was performed by rotary evaporation at 23–40 °C at an appropriate pressure. Final products were purified by Grace Reveleris X2 Column chromatography using Grace Reveleris Silica cartridges (12g or 40g). Purified compounds were further dried under vacuum (10^{-6}–10^{-3} bar). Yields refer to purified and spectroscopically pure compounds.

Aqueous ^{18}F-fluoride used in this work was produced by the ^{18}O(p,n)^{18}F nuclear reaction in an IBA (Louvain-la-Neuve, Belgium) Cyclone 18/9 cyclotron. Manual radiolabeling was performed in radiochemistry fume hoods at negative air pressure with respect to the laboratory. Radiolabeled products were monitored and identified by radio-TLC and radio-HPLC.

All animal procedures were carried out following the European Union directives for animal experiments (86/609/CEE, 2003/65/CE, and 2010/63/EU), and the protocols used (AVD105002016395 for mice works, and AVD10500201581 for guinea pig works) were previously approved by the Dutch National Committee on Animal Experiments and the Institutional Animal Care and User Committee of the University of Groningen.

8 male Dunkin Hartley guinea pigs (Envigo, Netherlands) weighing approximately 250 grams at the time of sensitization were used. The guinea pigs were housed conventionally in pairs, in ventilated cages in rooms maintained at a 12 hour light/dark cycle, and were provided *ad libitum* access to food and water.

32 immunocompromised male mice (6-8 weeks old BALB/c nude mice supplied by Envigo, Netherlands) were used. The animals were provided with sterilized chow and water *ad libitum*, and housed in individually ventilated cages equipped with a negative-pressure HEPA filtered air system. During tumor inoculation or PET scanning, the mice were anesthetized with isoflurane (5% for induction and 2% for maintenance).

Animals were scanned at least five days after the inoculation when the tumor reached a volume between 0.3 and 0.6 cm^3. Tumor diameters were measured 1 to 3 times per week with a caliper, and tumor volume was calculated using the following formula: $V_{tumor} = ab^2/2$, where *a* and *b* represent tumor length and width, respectively).

Spectroscopy and Instruments

High-resolution mass spectra (HRMS) were obtained using electrospray ionization (ESI) mass spectra (MS) system from Waters Investigator Semi-prep 15 Super Critical Fluid Chromatography (SFC) with a 3100 MS-ESI detector using a solvent system of methanol (with ammonium hydroxide as an additive) and CO_2 on an ethyl pyridine 4.6x250 mm column or from the taken TLC-SG plate using an Advion plate express TLC-MS. Semi-preparative high-performance liquid chromatography (HPLC) was performed on a Waters system using a 1525 binary HPLC pump, a 2489 UV/visible detector and a Berthold Technologies Flowstar LB 513 radio flow detector. Analytical analysis of the synthesized radiotracers for assessment of final quality control (QC) was acquired using a Waters Acquity integrated system coupled to a Berthold Technologies Flowstar LB 513 radio flow detector. HPLC data were processed with Waters Empower 3 software. Radio-TLC's were scanned using a Perkin Elmer Packard Cyclone storage phosphor system and the acquired data analyzed with the OptiQuant 03.00 software. Gamma-counting was performed on a Perkin Elmer Wallac Wizard 1470 (Turku, Finland), with an open energy window (15-1000 keV) and 15 seconds of measuring time.

Nuclear magnetic resonance (NMR) spectra were recorded on a Bruker 500 spectrometer operating at 500 MHz and 126 MHz for ^{1}H and ^{13}C acquisitions, respectively, in deuterated solvents. For ^{1}H NMR, chemical shifts (δ) are reported in ppm, with the solvent residual peak as the internal standard, and coupling constants (J) in hertz (Hz). The following abbreviations were used for spin multiplicity: s = singlet, d = doublet, t = triplet, q = quartet, m = multiplet. Chemical shifts for ^{13}C NMR were reported in ppm relative to the solvent peak.

mRNA Isolation and PCR Analysis

Total mRNA was isolated using Trizol RNA extraction (TRI Reagent Solution, Applied Biosystems, Landsmeer, Netherlands), according to the manufacturer's instructions. cDNA was synthesized from equal amounts of RNA using Reverse Transcriptase System (Promega, Madison, WI, USA), and the following protocol: 10 min 25°C, 45 min 42°C, 5 min 99°C. rtPCR was performed with SYBR Green (Roche Diagnostics, Almere, Netherlands) and the following protocol including a final step to generate the melting curve: 2 min 95°C, 10 min 95 °C, 45× (30 s 95°C, 30 s 60°C, 30 s 72°C), 30 s 95°C, 30 s 55°C, 30 s 95°C. The rtPCR was performed in an Eco Illumina (Illumina, Eindhoven, Netherlands). For analysis, the LinReg software was used to calculate N0-values, which were normalized to N0 of the housekeeping genes HPRT1 and GAPDH as an internal control. Primer sets used to analyze gene expression are:

Gene:	Forward primer	Reverse primer:
HPRT1	AAGCCAGACTTTGTTGGATT	ACTGGCGATGTCAATAGGAC
GAPDH	CCAGCAAGAGCACAAGAGGA	GAGATTCAGTGTGGTGGGGG
ARG1	GGAGACCACAGTTTGGCAAT	CCACTTGTGGTTGTCAGTGG
ARG2	TGCATCCTTGAACTGTCAGC	ACAAGCTGCTGCTTTCCATT

Surface Plasmon Resonance

Binding kinetics of the inhibitors were determined by surface plasmon resonance using a Biacore T200 (GE Healthcare). Arg1 was immobilized on a Ni-nitrilotriacetic acid sensor chip by Ni-mediated affinity capturing and amine-coupling to a level of 4000 or 6000 resonance units using 60 µg/mL Arg1 in running buffer (50 mM Na$_2$HPO$_4$, pH 7.4,150 mM KCl, and 0.01% Tween-20). The arginase inhibitors were diluted in the same running buffer and were injected in an increasing concentration range of 0.1, 0.316, 1.0, 3.16, and 10 µM. Single-cycle kinetics were used for measuring compound binding with a flow rate of 30 µL/min, an association time of 100 s per injection, and a dissociation time of 1800 s. The compound response was subtracted with both the reference channel response and the blank injection. The Biacore Evaluation software was used to fit the data to the Langmuir 1:1 binding model, with x^2 values indicating minimal deviation between the fit and the experimental data. This minimal deviation was confirmed by determination of the reliability of the curve fits with standard Biacore checks. All combinations of the inhibitors and pH conditions were measured in at least two technical replicates to determine the kinetic constants k_a, k_d, and K_D. The target residence time (τ) was calculated from the k_d value using the formula $\tau = 1/k_d$.

PET Acquisition, Image Reconstruction, and Biological Half-life Calculation

The anesthetized animals were placed in the micro-PET table in a prone position, on top of a heating pad at 38°C to keep constant body temperature, stretched out as much as possible to minimize organ superposition and with the tumor in the field of view. Subsequently, a 90 minutes emission scan was acquired with a Focus 220 rodent scanner (Siemens/Concorde). Between the injection time and the beginning of the scan, an average time of 5 minutes has passed. After completion of the PET scan, a 10 minutes transmission scan with a ^{57}Co point source was obtained for the correction of scatter and attenuation of 511 keV photons by tissue.

For the micro-PET image analysis, all emission scans were iteratively reconstructed (OSEM2d, 4 iterations, 16 subsets) after being normalized and corrected for attenuation and radioactive decay. The list-mode data of the emission scans were separated into 24 frames (6x10s, 4x30s, 2x60s, 1x120s, 1x180s, 4x300s, and

6x600s). A three-dimensional volume of interest (VOI) was manually drawn by a single observer on the original data set, delineating the desired area on the summed PET images (0–90 min) using the PMOD software package (version 3.9; PMOD Technologies LLC). These VOIs were used to create the corresponding time-activity curves and to calculate standardized uptake values (SUV). A single exponential curve was fitted to the SUV time-activity curves (using values from 40 to 90 min) by an iterative nonlinear least-squares approach using GraphPad Prism version 6.01 for Windows (GraphPad Software, La Jolla, CA, USA) to calculate the biological half-life of the tracer.

Compound Synthesis and Characterization

2-amino-6-borono-2-(1-(4-chlorobenzyl)piperidin-4-yl)hexanoic acid (MARS)
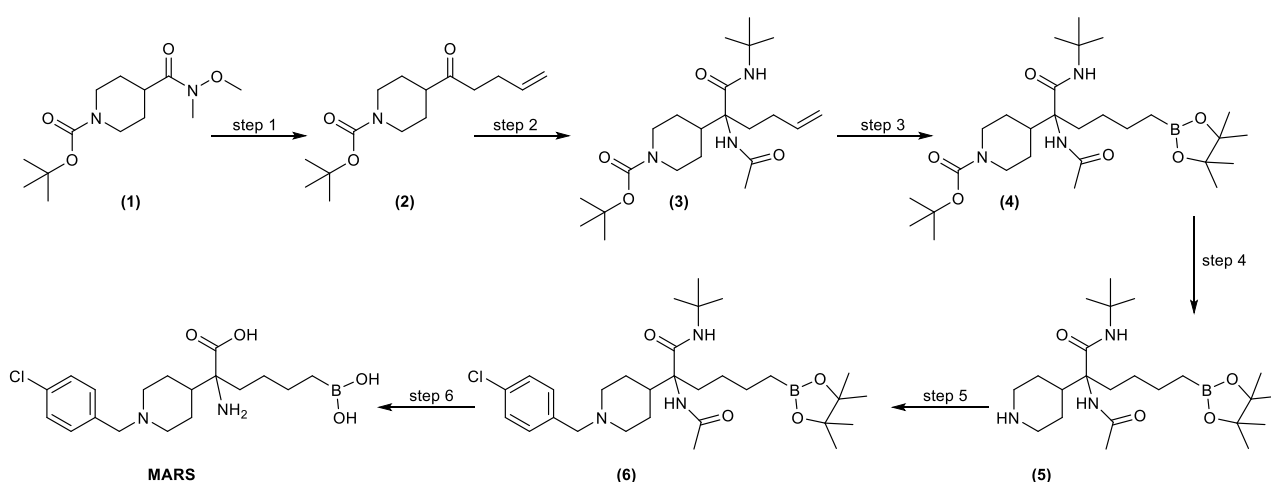
SCHEME 1. Synthesis pathway for the production of MARS.

Step 1: Activated metallic Mg (8.07 mmol, 2.20 eq.) and anhydrous THF (10 mL) were kept under nitrogen atmosphere. A pinch of iodine was added to initiate the reaction and to keep track of it as a red color became visible. 4-Bromobutene (7.34 mmol, 2.00 eq.) was then added dropwise to the reaction mixture. After 30 minutes the red color vanishes, indicating that most Mg was consumed and the Grignard reagents were formed. At this point, the Weinreb amide **1** (CAS 139290-70-3, 3.67 mmol, 1.00 eq.) was diluted in anhydrous THF (8 mL) in a different round bottom flask, flushed with nitrogen and cooled down to 0°C. The Grignard reagents previously produced were then transferred dropwise to the Weinreb amide solution. This mixture was left to stir for at least 30 minutes and the reaction followed by TLC-SG (15 % EtAc:DCM). After the reaction was confirmed to be complete, a saturated ammonium chloride solution was added. The THF layer was extracted, and the ammonium chloride solution was washed with another portion of THF. The combined organic layers were washed with sodium bicarbonate and dried to yield product **2** (74 %).

Step 2: The previously produced ketone **2** (7.48 mmol, 1.00 eq.) was added together with ammonium acetate (29.92 mmol, 4.00 eq.), 2,2,2-Trifluoroethanol (1 mL) and *tert*-butyl-isocyanide (14.96 mmol, 2.00 eq.). This mixture was left to stir for 10 days and followed by TLC-SG (10 % EtAc in DCM, ninhydrin) until the reaction mixture showed more product formed than starting material. At this point, the organic layer was washed with water, then with brine, dried with MgSO₄, filtrated, and evaporated at reduced pressure to yield the Ugi product **3** (48 %).

Step 3: 1,2-Bis(diphenylphosphino)ethane (dppe, 0.22 mmol, 0.03 eq.) and [Ir(cod)Cl]₂ (0.07 mmol, 0.01 eq.) were transferred to an oven-dried round bottom flask, kept under nitrogen atmosphere and anhydrous DCM (10 mL) added. This mixture was left to stir until a homogenous mixture was formed. To this mixture was added the previously formed Ugi product **3** (7.32 mmol, 1.00 eq.) dissolved in anhydrous DCM (20 mL). After 15 minutes, 4,4,5,5-tetramethyl-1,3,2-dioxaborolane (8.05 mmol, 1.10 eq.) was added with the round bottom

flask cooled down in a water bath (to prevent spontaneous heating). The reaction mixture was left to stir overnight at room temperature and followed by TLC-SG (50 % EtAc in PE, ninhydrin). The reaction mixture was slowly quenched with 3 mL of methanol and 30 mL of water. The aqueous layer was washed with DCM and the organic layer washed then with brine, dried with MgSO$_4$, and purified by flash chromatography to yield product **4** (59 %).

Step 4: Product **4** (4.28 mmol, 1.00 eq.) was dissolved in dioxane (10 mL). To this, 4N HCl in dioxane (17.12 mmol, 4.00 eq.) was added and the reaction mixture left to stir for 1 hour. The reaction was followed by TLC-SG (50 % EA in PE, ninhydrin). The mixture was then evaporated, dissolved in diethylether, and evaporated again to yield product **5** in its salt form (98 %).

Step 5: Salt **5** (0.42 mmol, 1.00 eq.) was dissolved in 1,2-dichloroethane (2 mL) and trimethylamine (0.42 mmol, 1.00 eq.) was added followed by 4-chlorobenzaldehyde (0.63 mmol, 1.50 eq.). The reaction mixture was left to stir for 1 hour and a first portion of sodium triacetoxyborohydride (0.53 mmol, 1.25 eq.) was added. This mixture was allowed to stir for 1 hour. Then a second portion of sodium triacetoxyborohydride (0.53 mmol, 1.25 eq.) was added and the mixture allowed to stir overnight. The reaction mixture was followed by TLC-SG (10 % MeOH in DCM, ninhydrin), washed with bicarbonate, and purified by flash chromatography to yield product **6** (70 %).

Step 6: Product **6** (0.18 mmol, 1.00 eq.) was dissolved in DCM (1 mL) and 4 mL of 6N HCl added. The mixture was refluxed overnight, and the aqueous layer was extracted and washed with DCM. The water was evaporated to yield the pure **MARS** product (98 %).


NMR spectroscopy of MARS

^{1}**H NMR** (500 MHz, CDCl$_3$) δ 7.48 (s, 2H), 7.44 (d, J = 8.1 Hz, 2H), 4.28 (s, 2H), 3.63 (s, 2H), 3.09 – 2.99 (m, 2H), 2.22 (t, J = 12.4 Hz, 1H), 2.13 (d, J = 14.2 Hz, 1H), 1.87 (d, J = 36.1 Hz, 3H), 1.59 – 1.48 (m, 1H), 1.42 – 1.39 (m, 1H), 1.33 (s, 8H), 1.17 (dq, J = 20.5, 7.3, 6.9 Hz, 1H), 0.76 (t, J = 7.6 Hz, 2H).

^{13}**C NMR** (126 MHz, CDCl$_3$) δ 172.07, 135.75, 132.89, 129.34, 127.02, 65.86, 62.65, 59.83, 52.08, 51.77, 38.53, 32.45, 26.75, 25.33, 23.98, 23.53, 13.85, 13.02.

HRMS-ESI: m/z [M-4+1H] (in presence of ammonium hydroxide) 379.10.

(5-acetamido-6-(*tert*-butylamino)-6-oxo-5-(1-(4-(4,4,5,5-tetramethyl-1,3,2-dioxaborolan-2-yl)benzyl) piperidin-4-yl)hexyl)boronic acid (FMARS arylboronic ester precursor)
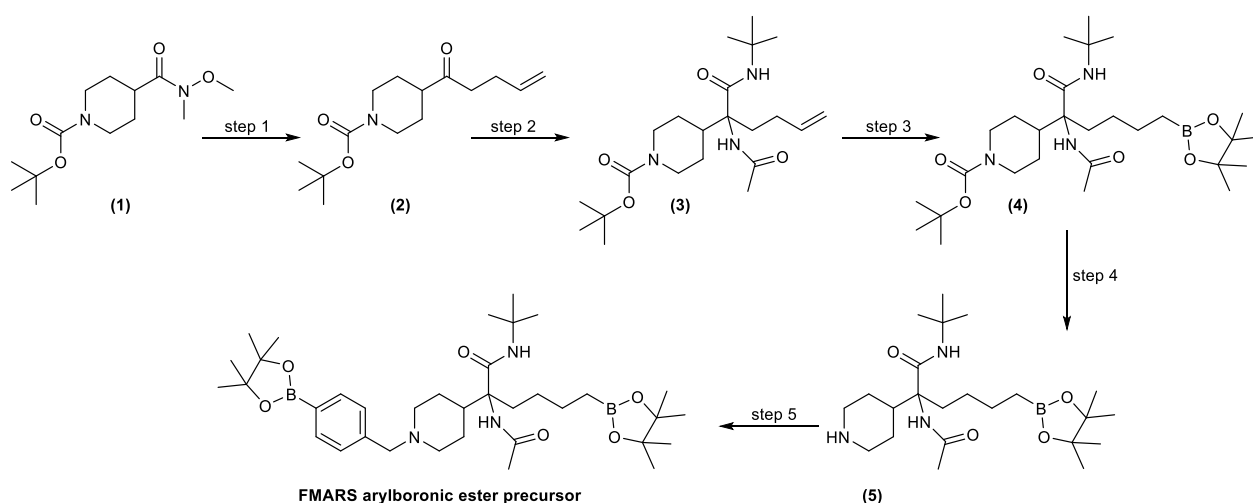
SCHEME 2. Synthesis pathway for the production of FMARS arylboronic ester precursor.

Step 1: Activated metallic Mg (8.07 mmol, 2.20 eq.) and anhydrous THF (10 mL) were kept under nitrogen atmosphere. A pinch of iodine was added to initiate the reaction and to keep track of it as a red color became visible. 4-Bromobutene (7.34 mmol, 2.00 eq.) was then added dropwise to the reaction mixture. After 30 minutes the red color vanishes, indicating that most Mg was consumed and the Grignard reagents were formed. At this point, the Weinreb amide **1** (CAS 139290-70-3, 3.67 mmol, 1.00 eq.) was diluted in anhydrous THF (8 mL) in a different round bottom flask, flushed with nitrogen and cooled down to 0°C. The Grignard reagents previously produced were then transferred dropwise to the Weinreb amide solution. This mixture was left to stir for at least 30 minutes and the reaction followed by TLC-SG (15 % EtAc:DCM). After the reaction was confirmed to be complete, a saturated ammonium chloride solution was added. The THF layer was extracted and the ammonium chloride solution washed with another portion of THF. The combined organic layers were washed with sodium bicarbonate and dried to yield product **2** (74 %).

Step 2: The previously produced ketone **2** (7.48 mmol, 1.00 eq.) was added together with ammonium acetate (29.92 mmol, 4.00 eq.), 2,2,2-Trifluoroethanol (1 mL) and *tert*-butyl-isocyanide (14.96 mmol, 2.00 eq.). This mixture was left to stir for 10 days and followed by TLC-SG (10 % EtAc in DCM, ninhydrin) until the reaction mixture showed more product formed than starting material. At this point, the organic layer was washed with water, then with brine, dried with MgSO$_4$, filtrated, and evaporated at reduced pressure to yield the Ugi product **3** (48 %).

Step 3: 1,2-Bis(diphenylphosphino)ethane (dppe, 0.22 mmol, 0.03 eq.) and [Ir(cod)Cl]$_2$ (0.07 mmol, 0.01 eq.) were transferred to an oven-dried round bottom flask, kept under nitrogen atmosphere and anhydrous DCM (10 mL) added. This mixture was left to stir until a homogenous mixture was formed. To this mixture was added the previously formed Ugi product **3** (7.32 mmol, 1.00 eq.) dissolved in anhydrous DCM (20 mL). After 15 minutes, 4,4,5,5-tetramethyl-1,3,2-dioxaborolane (8.05 mmol, 1.10 eq.) was added with the round bottom flask cooled down in a water bath (to prevent spontaneous heating). The reaction mixture was left to stir overnight at room temperature and followed by TLC-SG (50 % EtAc in PE, ninhydrin). The reaction mixture was slowly quenched with 3 mL of methanol and 30 mL of water. The aqueous layer was washed with DCM and the organic layer washed then with brine, dried with MgSO$_4$, and purified by flash chromatography to yield product **4** (59 %).

Step 4: Product **4** (4.28 mmol, 1.00 eq.) was dissolved in dioxane (10 mL). To this, 4N HCl in dioxane (17.2 mmol, 4.00 eq.) was added and the reaction mixture left to stir for 1 hour. The reaction was followed by TLC-SG (50 % EA in PE, ninhydrin). The mixture was then evaporated, dissolved in diethylether, and evaporated again to yield product **5** in its salt form (98 %).

Step 5: Salt **5** (0.42 mmol, 1.00 eq.) and K$_2$CO$_3$ (0.84 mmol, 2.00 eq.) were dissolved in DMF (2 mL). This mixture was left stirring for a few minutes to obtain the free base, which can be observed by a color change from grey to green. At this point, 4-bromomethylphenylboronic acid pinacol ester (0.46 mmol, 1.10 eq.) was added and left to stir for 2 hours. The reaction was followed by TLC-SG (5 % MeOH in DCM, ninhydrin). The reaction mixture was then poured on ice to induce precipitation and then filtered. The collected product was washed with water and dried to yield the **FMARS arylboronic ester precursor** as a white solid (68 %).


NMR spectroscopy of FMARS arylboronic ester precursor

^{1}H NMR (500 MHz, CDCl$_3$) δ 7.74 (d, *J* = 7.8 Hz, 2H), 7.28 (d, *J* = 7.7 Hz, 2H), 6.93 (s, 1H), 5.53 (s, 1H), 3.56 – 3.39 (m, 2H), 2.87 (d, *J* = 5.6 Hz, 3H), 2.08 (t, *J* = 6.1 Hz, 1H), 1.97 (s, 3H), 1.95 – 1.82 (m, 2H), 1.71 (s, 4H), 1.58 (d, *J* = 27.2 Hz, 1H), 1.35 (d, *J* = 13.2 Hz, 25H), 1.22 (s, 11H), 1.08 – 0.95 (m, 1H), 0.73 (t, *J* = 7.9 Hz, 2H).

^{13}C NMR (126 MHz, CDCl$_3$) δ 171.02, 170.99, 169.17, 169.07, 141.70, 141.65, 134.73, 128.57, 83.80, 83.03, 66.67, 66.60, 63.11, 54.10, 53.81, 51.91, 42.82, 42.73, 32.11, 31.97, 28.85, 27.69, 27.45, 26.92, 26.33, 24.97, 24.93, 24.89, 24.74, 24.72, 24.28, 22.86, 14.13.

HRMS-ESI: m/z [M+H]$^+$ 654.48.

2-amino-6-borono-2-(1-(4-fluorobenzyl)piperidin-4-yl)hexanoic acid (FMARS)
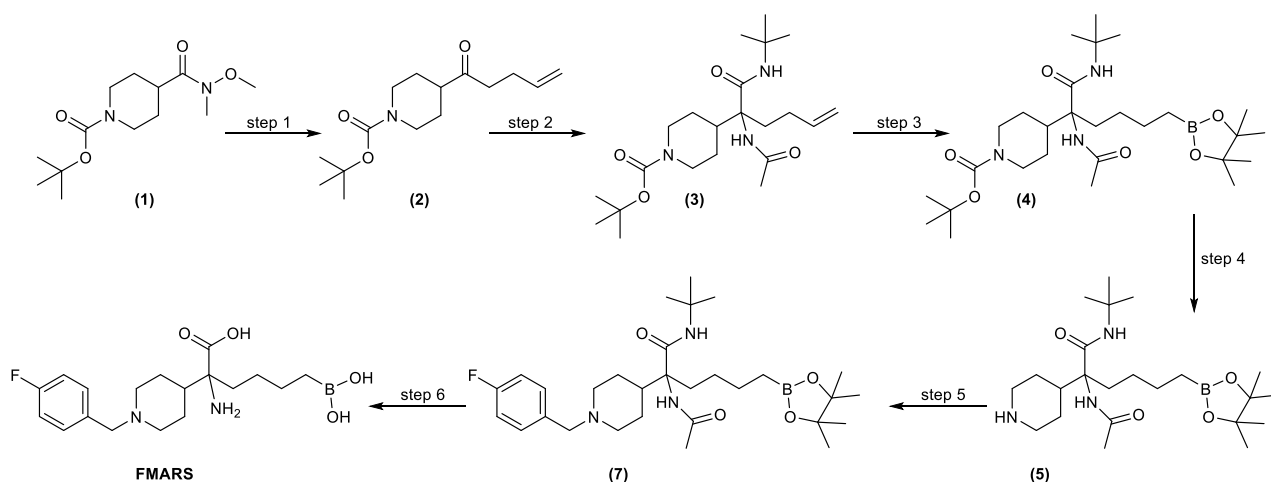
SCHEME 3. Synthesis pathway for the production of FMARS.

Step 1: Activated metallic Mg (8.07 mmol, 2.20 eq.) and anhydrous THF (10 mL) were kept under nitrogen atmosphere. A pinch of iodine was added to initiate the reaction and to keep track of it as a red color became visible. 4-Bromobutene (7.34 mmol, 2.00 eq.) was then added dropwise to the reaction mixture. After 30 minutes the red color vanishes, indicating that most Mg was consumed and the Grignard reagents were formed. At this point, the Weinreb amide **1** (CAS 139290-70-3, 3.67 mmol, 1.00 eq.) was diluted in anhydrous THF (8 mL) in a different round bottom flask, flushed with nitrogen and cooled down to 0°C. The Grignard reagents previously produced were then transferred dropwise to the Weinreb amide solution. This mixture was left to stir for at least 30 minutes and the reaction followed by TLC-SG (15 % EtAc:DCM). After the reaction was confirmed to be complete, a saturated ammonium chloride solution was added. The THF layer was extracted and the ammonium chloride solution washed with another portion of THF. The combined organic layers were washed with sodium bicarbonate and dried to yield product **2** (74 %).

Step 2: The previously produced ketone **2** (7.48 mmol, 1.00 eq.) was added together with ammonium acetate (29.92 mmol, 4.00 eq.), 2,2,2-Trifluoroethanol (1 mL) and *tert*-butyl-isocyanide (14.96 mmol, 2.00 eq.). This mixture was left to stir for 10 days and followed by TLC-SG (10 % EtAc in DCM, ninhydrin) until the reaction mixture showed more product formed than starting material. At this point, the organic layer was washed with water, then with brine, dried with $MgSO_4$, filtrated, and evaporated at reduced pressure to yield the Ugi product **3** (48 %).

Step 3: 1,2-Bis(diphenylphosphino)ethane (dppe, 0.22 mmol, 0.03 eq.) and [Ir(cod)Cl]$_2$ (0.07 mmol, 0.01 eq.) were transferred to an oven-dried round bottom flask, kept under nitrogen atmosphere and anhydrous DCM (10 mL) added. This mixture was left to stir until a homogenous mixture was formed. To this mixture was added the previously formed Ugi product **3** (7.32 mmol, 1.00 eq.) dissolved in anhydrous DCM (20 mL). After 15 minutes, 4,4,5,5-tetramethyl-1,3,2-dioxaborolane (8.05 mmol, 1.10 eq.) was added with the round bottom flask cooled down in a water bath (to prevent spontaneous heating). The reaction mixture was left to stir overnight at room temperature and followed by TLC-SG (50 % EtAc in PE, ninhydrin). The reaction mixture was slowly quenched with 3 mL of methanol and 30 mL of water. The aqueous layer was washed with DCM and the organic layer washed then with brine, dried with $MgSO_4$, and purified by flash chromatography to yield product **4** (59 %).

Step 4: Product **4** (4.28 mmol, 1.00 eq.) was dissolved in dioxane (10 mL). To this, 4N HCl in dioxane (17.12 mmol, 4.00 eq.) was added and the reaction mixture left to stir for 1 hour. The reaction was followed by TLC-SG (50 % EA in PE, ninhydrin). The mixture was then evaporated, dissolved in diethylether, and evaporated again to yield product **5** in its salt form (98 %).

Step 5: Salt **5** (0.42 mmol, 1.00 eq.) was dissolved in 1,2-dichloroethane (2 mL) and trimethylamine (0.42 mmol, 1.00 eq.) was added followed by 4-fluorobenzaldehyde (0.63 mmol, 1.50 eq.). The reaction mixture was left to stir for 1 hour and a first portion of sodium triacetoxyborohydride (0.53 mmol, 1.25 eq.) was added. This mixture was allowed to stir for 1 hour, and then a second portion of sodium triacetoxyborohydride (0.53 mmol, 1.25 eq.) was added and the mixture allowed to stir overnight. The reaction mixture was followed by TLC-SG (10 % MeOH in DCM, ninhydrin), washed with bicarbonate, and purified by flash chromatography to yield product **7** (70 %).

Step 6: Product **7** (0.18 mmol, 1.00 eq.) was dissolved in DCM (1 mL) and 4 mL of 6N HCl added. The mixture was refluxed overnight, and the aqueous layer was extracted and washed with DCM. The water was evaporated to yield the pure **FMARS** product (98 %).

NMR spectroscopy of FMARS

^{1}**H NMR** (500 MHz, D$_2$O) δ 7.42 (dd, J = 8.5, 5.2 Hz, 2H), 7.14 (t, J = 8.6 Hz, 2H), 4.22 (s, 2H), 3.54 (d, J = 10.9 Hz, 1H), 2.98 (qd, J = 6.1, 2.9 Hz, 1H), 2.17 (tt, J = 12.7, 3.2 Hz, 1H), 2.07 (dt, J = 14.0, 2.9 Hz, 1H), 1.87 (d, J = 19.0 Hz, 2H), 1.82 – 1.70 (m, 1H), 1.48 (qd, J = 13.1, 3.9 Hz, 1H), 1.37 – 1.30 (m, 2H), 1.27 (s, 9H), 1.10 (dt, J = 25.5, 7.0 Hz, 1H), 0.69 (t, J = 7.6 Hz, 2H).

^{13}**C NMR** (126 MHz, CDCl$_3$) δ 174.93, 167.09, 165.12, 136.08, 136.01, 127.03, 118.80, 118.62, 68.59, 62.41, 54.26, 54.18, 41.17, 35.11, 29.24, 27.89, 26.59, 26.12.

HRMS-ESI: m/z [M-4+1H] (in presence of ammonium hydroxide) 363.26.

(5-acetamido-6-(*tert*-butylamino)-6-oxo-5-(3-(4-(4,4,5,5-tetramethyl-1,3,2-dioxaborolan-2-yl)benzyl)-3-azabicyclo[3.2.1]octan-8-yl)hexyl)boronic acid (FBMARS arylboronic ester precursor)
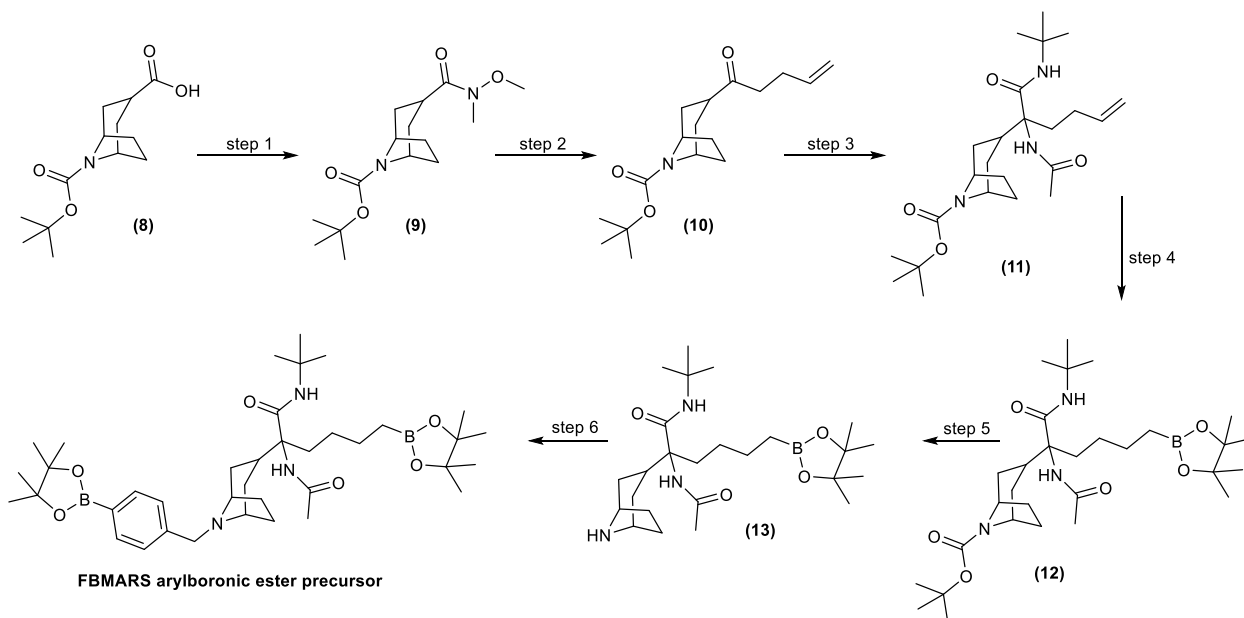
SCHEME 4. Synthesis pathway for the production of FBMARS arylboronic ester precursor.

Step 1: Compound **8** (CAS 280762-00-7, 16.00 mmol, 1.00 eq.) and hydroxybenzotriazole (19.20 mmol, 1.20 eq.) were kept under nitrogen atmosphere in a round bottom flask. To this, it was added DCM (78 mL), trimethylamine (48.00 mmol, 3.00 eq.) and, after 5 minutes, N,O-hydroxyalamine hydrochloride (24.00 mmol, 1.50 eq.). The mixture was then left to stir at room temperature for 30 minutes, and then 1-ethyl-3-(3-dimethylaminopropyl)carbodiimide (24.00 mmol, 1.50 eq.) was added. The reaction mixture was left to stir

overnight, and the reaction followed by TLC-SG (20 % EtAc in PE, ninhydrin). After the starting material completely vanishes from the TLC-SG profile, the reaction was quenched with 100 mL of water and 50 mL DCM was added. The organic layer was washed with 1N HCl and then with sodium bicarbonate. The product was then dried under high pressure and crystallized overnight to form the Weinreb amide **9** as a white solid (96 %).

Step 2: Activated metallic Mg (33.00 mmol, 2.20 eq.) and anhydrous THF (40 mL) were kept under nitrogen atmosphere. A pinch of iodine was added to initiate the reaction and to keep track of it as a red color became visible. 4-Bromobutene (10.50 mmol, 0.70 eq.) was then added dropwise to the reaction mixture. After 30 minutes a second portion of 4-bromobutene (21.00 mmol, 1.40 eq.) is added and left to stir for further 30 minutes until the red color vanishes, indicating that most Mg was consumed and the Grignard reagents were formed. At this point, the Weinreb amide **9** (15.00 mmol, 1.00 eq.) was diluted in anhydrous THF (40 mL) in a different round bottom flask, flushed with nitrogen and stirred overnight. The reaction was followed by TLC-SG (15 % EtAc in DCM, ninhydrin). After the reaction was confirmed to be complete, a saturated ammonium chloride solution was added. The THF layer was extracted and the ammonium chloride solution washed with another portion of THF. The combined organic layers were washed with sodium bicarbonate and dried to yield product **10** (99 %).

Step 3: The previously produced ketone **10** (3.30 mmol, 1.00 eq.) was added together with ammonium acetate (13.20 mmol, 4.00 eq.), 2,2,2-Trifluoroethanol (1 mL) and *tert*-butyl-isocyanide (6.60 mmol, 2.00 eq.). This mixture was left to stir for 3 weeks and followed by TLC-SG (10 % EtAc in DCM, ninhydrin) until the reaction mixture showed more product formed than starting material. At this point, the organic layer was washed with water, dried with $MgSO_4$, and purified by flash chromatography to yield the Ugi product **11** (57 %).

Step 4: 1,2-Bis(diphenylphosphino)ethane (dppe, 0.07 mmol, 0.03 eq.) and $[Ir(cod)Cl]_2$ (0.02 mmol, 0.01 eq.) were transferred to an oven-dried round bottom flask, kept under nitrogen atmosphere and anhydrous DCM (6.5 mL) added. This mixture was left to stir until a homogenous mixture was formed. To this mixture was added the previously formed Ugi product **11** (2.30 mmol, 1.00 eq.) dissolved in anhydrous DCM (6 mL). After 15 minutes, 4,4,5,5-tetramethyl-1,3,2-dioxaborolane (2.50 mmol, 1.10 eq.) was added with the round bottom flask cooled down in a water bath (to prevent spontaneous heating). The reaction mixture was left to stir overnight at room temperature and followed by TLC-SG (50 % EtAc in PE, ninhydrin). The reaction mixture was slowly quenched with 0.5 mL of methanol and 10 mL of water. The aqueous layer was washed with DCM and the organic layer washed then with brine, dried with $MgSO_4$, and purified by flash chromatography to yield product **12** (73 %).

Step 5: Product **12** (2.70 mmol, 1.00 eq.) was dissolved in dioxane (5 mL). To this, 4N HCl in dioxane (10.80 mmol, 4.00 eq.) was added and the reaction mixture left to stir for 1 hour. The reaction was followed by TLC-SG (50 % EA in PE, ninhydrin). The mixture was then evaporated to yield **13** as a withe solid in its salt form (95 %).

Step 6: Salt **13** (0.42 mmol, 1.00 eq.) and K_2CO_3 (0.84 mmol, 2.00 eq.) were dissolved in DMF (2 mL). This was left stirring for a few minutes to obtain the free base, which can be observed by a color change from grey to green. At this point, 4-bromomethylphenylboronic acid pinacol ester (0.46 mmol, 1.10 eq.) was added and left to stir overnight. The reaction was followed by TLC-SG (5 % MeOH in DCM, ninhydrin). The reaction mixture was then poured on ice to induce precipitation and then filtered. The collected product was washed with water and dried to yield the **FBMARS arylboronic ester** precursor as a white solid (71 %).


NMR spectroscopy of FBMARS arylboronic ester

^{1}H NMR (500 MHz, CDCl$_3$) δ 7.73 (d, *J* = 7.8 Hz, 2H), 7.35 (d, *J* = 7.7 Hz, 2H), 6.91 (s, 1H), 5.71 (s, 1H), 3.52 (s, 1H), 3.17 (s, 1H), 2.73 (t, *J* = 11.1 Hz, 1H), 2.64 (dt, *J* = 12.5, 6.9 Hz, 1H), 2.02 – 1.92 (m, 5H),

1.63 – 1.54 (m, 3H), 1.50 (d, J = 11.3 Hz, 2H), 1.40 (s, 12H), 1.34 (s, 16H), 1.22 (s, 13H), 0.73 (t, J = 7.8 Hz, 2H).

^{13}C NMR (126 MHz, CDCl$_3$) δ 171.27, 169.20, 143.77, 134.84, 134.70, 127.86, 83.79, 83.02, 66.84, 59.31, 58.95, 58.46, 56.32, 51.82, 36.59, 34.06, 32.83, 32.46, 32.23, 31.55, 28.98, 28.89, 26.95, 26.78, 26.54, 25.03, 24.99, 24.96, 24.93, 24.90, 24.87, 24.69, 24.63, 24.33.

HRMS-ESI: m/z [M+H]$^+$ 680.49.

2-amino-6-borono-2-(3-(4-fluorobenzyl)-3-azabicyclo[3.2.1]octan-8-yl)hexanoic acid (FBMARS)
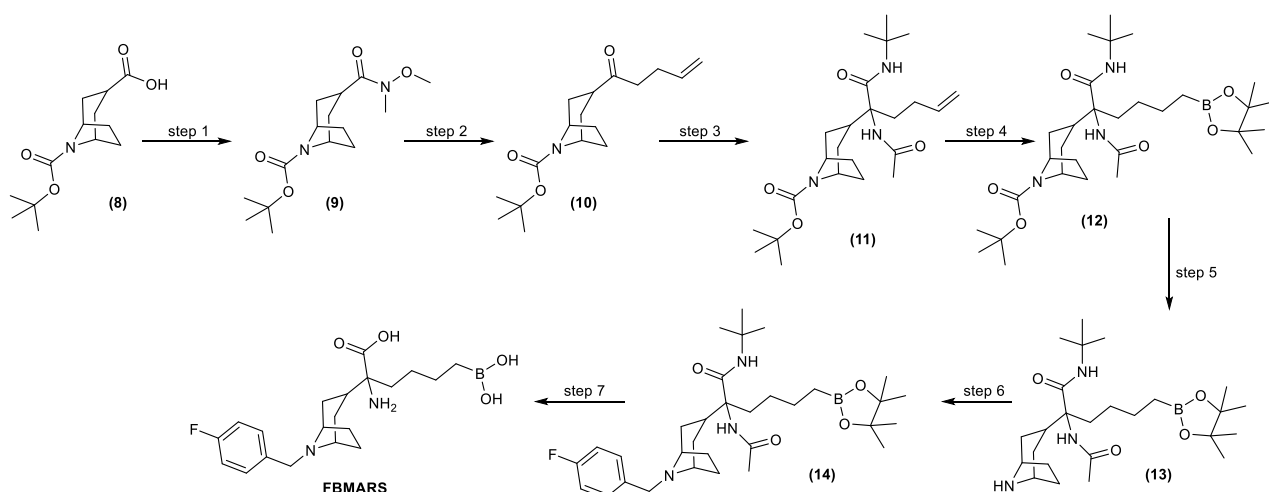
SCHEME 5. Synthesis pathway for the production of FBMARS

Step 1: Compound **8** (CAS 280762-00-7, 16.00 mmol, 1.00 eq.) and hydroxybenzotriazole (19.20 mmol, 1.20 eq.) were kept under nitrogen atmosphere in a round bottom flask. To this, it was added DCM (78 mL), trimethylamine (48.00 mmol, 3.00 eq.) and, after 5 minutes, N,O-hydroxyalamine hydrochloride (24.00 mmol, 1.50 eq.). The mixture was then left to stir at room temperature for 30 minutes and then 1-ethyl-3-(3-dimethylaminopropyl)carbodiimide (24.00 mmol, 1.50 eq.) was added. The reaction mixture was left to stir overnight, and the reaction followed by TLC-SG (20 % EtAc in PE, ninhydrin). After the starting material completely vanishes from the TLC-SG profile, the reaction was quenched with 100 mL of water and 50 mL DCM was added. The organic layer was washed with 1N HCl and then with sodium bicarbonate. The product was then dried under high pressure and crystallized overnight to form the Weinreb amide **9** as a white solid (96 %).

Step 2: Activated metallic Mg (33.00 mmol, 2.20 eq.) and anhydrous THF (40 mL) were kept under nitrogen atmosphere. A pinch of iodine was added to initiate the reaction and to keep track of it as a red color became visible. 4-Bromobutene (10.50 mmol, 0.70 eq.) was then added dropwise to the reaction mixture. After 30 minutes a second portion of 4-bromobutene (21.00 mmol, 1.40 eq.) is added and left to stir for further 30 minutes until the red color vanishes, indicating that most Mg was consumed and the Grignard reagents were formed. At this point, the Weinreb amide **9** (15.00 mmol, 1.00 eq.) was diluted in anhydrous THF (40 mL) in a different round bottom flask, flushed with nitrogen and stirred overnight. The reaction was followed by TLC-SG (15 % EtAc in DCM, ninhydrin). After the reaction was confirmed to be complete, a saturated ammonium chloride solution was added. The THF layer was extracted and the ammonium chloride solution washed with another portion of THF. The combined organic layers were washed with sodium bicarbonate and dried to yield product **10** (99 %).

Step 3: The previously produced ketone **10** (3.30 mmol, 1.00 eq.) was added together with ammonium acetate (13.20 mmol, 4.00 eq.), 2,2,2-Trifluoroethanol (1 mL) and *tert*-butyl-isocyanide (6.60 mmol, 2.00 eq.). This mixture was left to stir for 3 weeks and followed by TLC-SG (10 % EtAc in DCM, ninhydrin) until the

reaction mixture showed more product formed than starting material. At this point, the organic layer was washed with water, dried with MgSO₄, and purified by flash chromatography to yield the Ugi product **11** (57 %).

Step 4: 1,2-Bis(diphenylphosphino)ethane (dppe, 0.07 mmol, 0.03 eq.) and [Ir(cod)Cl]₂ (0.02 mmol, 0.01 eq.) were transferred to an oven-dried round bottom flask, kept under nitrogen atmosphere and anhydrous DCM (6.5 mL) added. This mixture was left to stir until a homogenous mixture was formed. To this mixture was added the previously formed Ugi product **11** (2.30 mmol, 1.00 eq.) dissolved in anhydrous DCM (6 mL). After 15 minutes, 4,4,5,5-tetramethyl-1,3,2-dioxaborolane (2.50 mmol, 1.10 eq.) was added with the round bottom flask cooled down in a water bath (to prevent spontaneous heating). The reaction mixture was left to stir overnight at room temperature and followed by TLC-SG (50 % EtAc in PE, ninhydrin). The reaction mixture was slowly quenched with 0.5 mL of methanol and 10 mL of water. The aqueous layer was washed with DCM and the organic layer washed then with brine, dried with MgSO₄, and purified by flash chromatography to yield product **12** (73 %).

Step 5: Product **12** (2.70 mmol, 1.00 eq.) was dissolved in dioxane (5 mL). To this, 4N HCl in dioxane (10.80 mmol, 4.00 eq.) was added and the reaction mixture left to stir for 1 hour. The reaction was followed by TLC-SG (50 % EA in PE, ninhydrin). The mixture was then evaporated to yield **13** as a withe solid in its salt form (95 %).

Step 6: Salt **13** (0.43 mmol, 1.00 eq.) was dissolved in 1,2-dichloroethane (2 mL) and trimethylamine (0.43 mmol, 1.00 eq.) was added followed by 4-fluorobenzaldehyde (0.65 mmol, 1.50 eq.). The reaction mixture was left to stir for 1 hour and a first portion of sodium triacetoxyborohydride (0.54 mmol, 1.25 eq.) was added. This mixture was allowed to stir for 1 hour, and then a second portion of sodium triacetoxyborohydride (0.54 mmol, 1.25 eq.) was added and the mixture allowed to stir overnight. The reaction mixture was followed by TLC-SG (10 % MeOH in DCM, ninhydrin), washed with bicarbonate, and purified by flash chromatography to yield product **14** (54 %).

Step 7: Product **14** (0.21 mmol, 1.00 eq.) was dissolved in DCM (1 mL) and 4 mL of 6N HCl added. The mixture was refluxed overnight and the aqueous layer extracted and washed with DCM. The water was evaporated to yield the pure **FBMARS** product (95 %).


NMR spectroscopy of FBMARS

¹H NMR (500 MHz, CD₃OD) δ 7.73 – 7.56 (m, 2H), 7.23 (td, J = 8.6, 2.6 Hz, 2H), 4.21 (d, J = 11.5 Hz, 2H), 4.06 – 3.92 (m, 2H), 2.50 (d, J = 34.2 Hz, 3H), 2.33 – 2.18 (m, 1H), 2.09 (q, J = 10.5, 9.7 Hz, 3H), 2.03 – 1.74 (m, 4H), 1.44 (d, J = 12.5 Hz, 2H), 1.37 (d, J = 2.6 Hz, 7H), 1.24 (d, J = 12.6 Hz, 1H), 0.76 (s, 1H).

¹³C NMR (126 MHz, D₂O) δ 172.44, 164.42, 162.45, 132.95, 125.14, 116.26, 65.92, 61.24, 60.97, 60.70, 54.13, 51.94, 48.83, 46.71, 32.37, 29.86, 26.59, 25.25, 23.43, 12.84.

HRMS-ESI: m/z [M-4+1H] (in presence of ammonium hydroxide) 389.3.

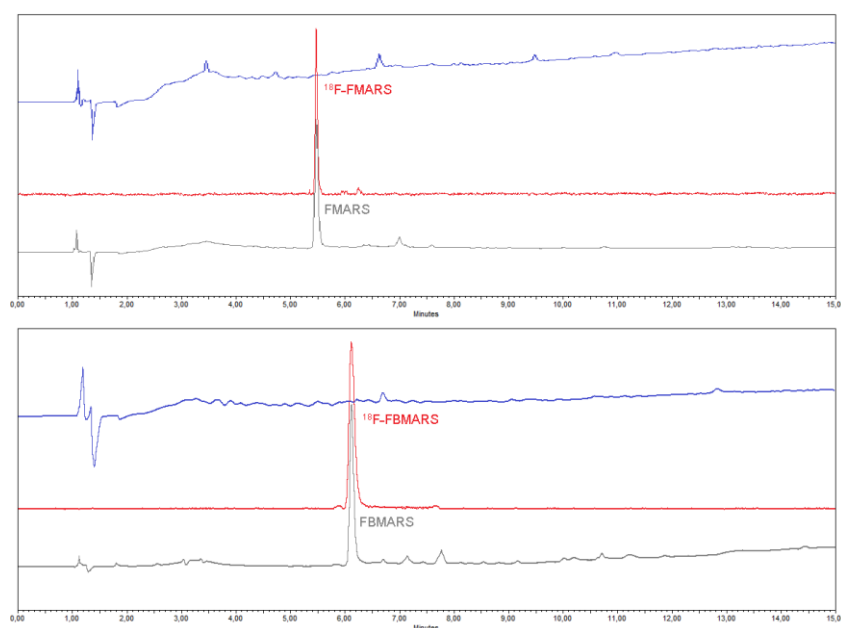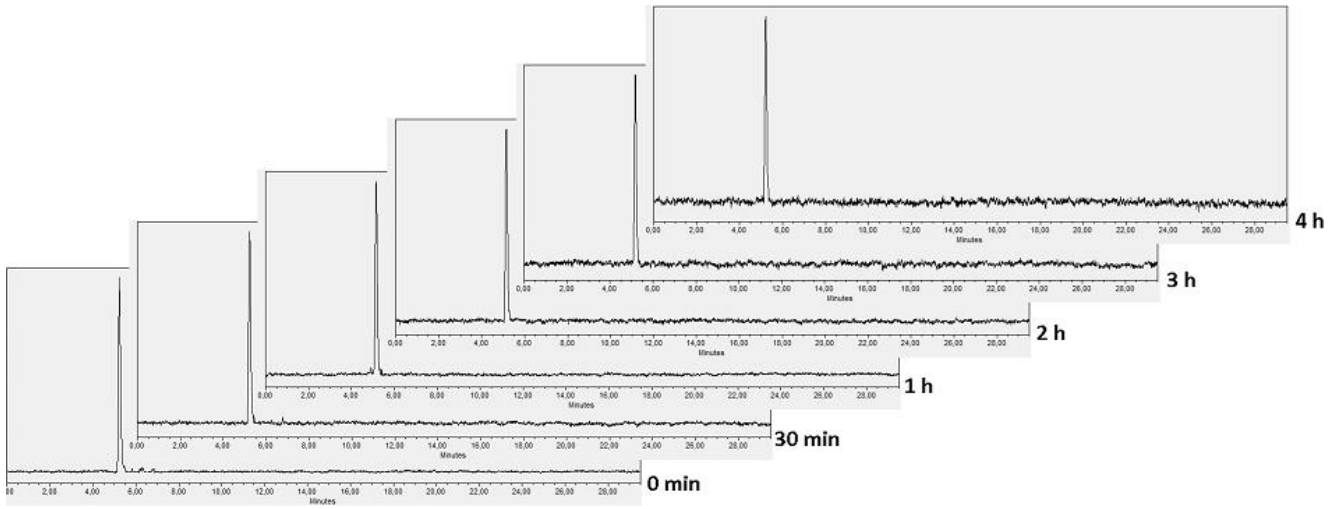# Supplementary Figures
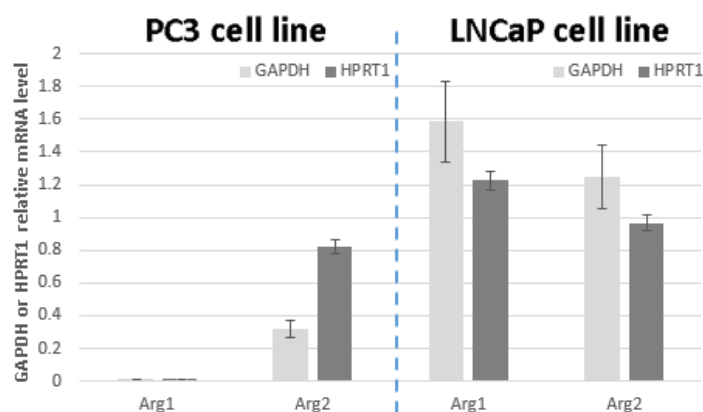
SUPPLEMENTAL FIGURE 1. Arg1 and Arg2 mRNA expression levels normalized with GAPDH and HPRT1 reference (housekeeping) genes in the used PC3 and LNCaP cell lines (n=3).
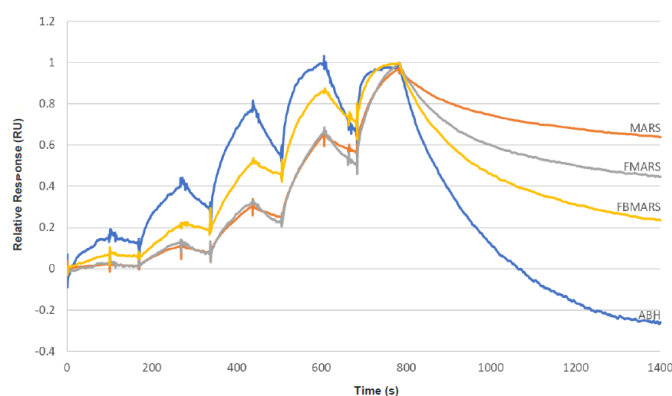

SUPPLEMENTAL FIGURE 2. Surface plasmon resonance sensorgrams (BiaCore T200) for Arg1 showing the binding of ABH, MARS, FMARS, and FBMARS (pH 7.4, inhibitor concentrations: 0.1-10 µM).
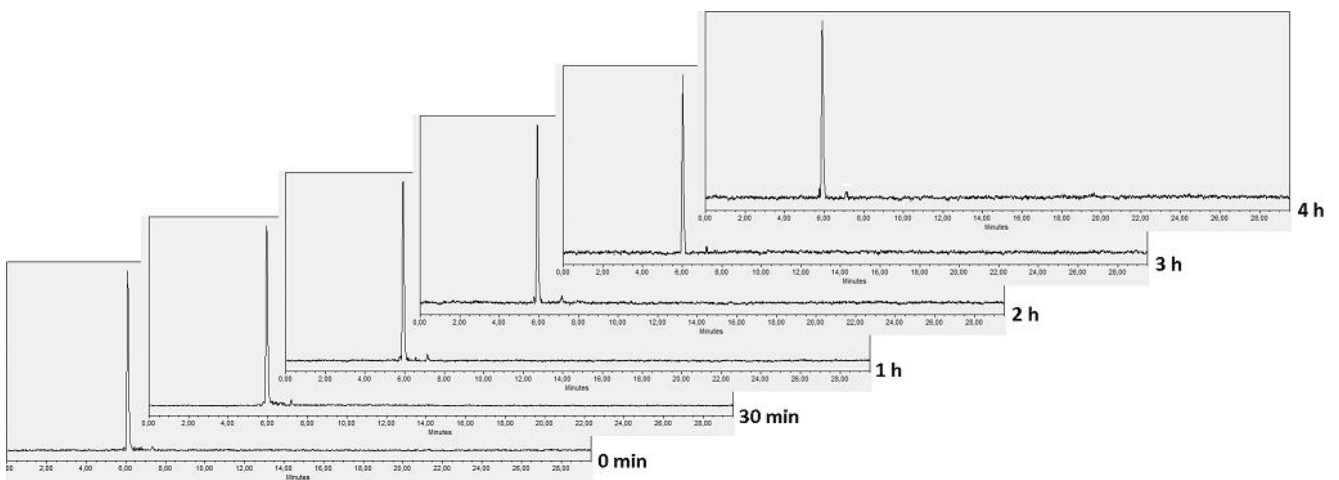

SUPPLEMENTAL FIGURE 3. Representative analytical HPLC profiles (blue, UV detector; red, γ detector) of ^{18}F-FMARS (top) and ^{18}F-FBMARS (bottom) with respective non-radioactive standards (gray UV signal).

11

SUPPLEMENTAL FIGURE 4. Representative radio-HPLC of the in vitro stability tests performed for ^{18}F-FMARS by incubating the radiotracers with serum at 37°C for up to 4 hours.
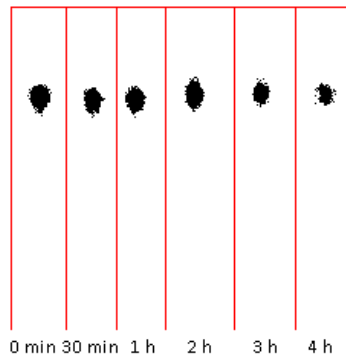

SUPPLEMENTAL FIGURE 5. Representative radio-TLC of the in vitro stability tests performed for ^{18}F-FMARS by incubating the radiotracers with serum at 37°C for up to 4 hours.

SUPPLEMENTAL FIGURE 6. Representative radio-HPLC of the in vitro stability tests performed for ^{18}F-FBMARS by incubating the radiotracers with serum at 37°C for up to 4 hours.
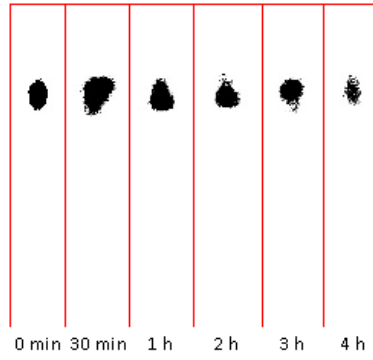
SUPPLEMENTAL FIGURE 7. Representative radio-TLC of the in vitro stability tests performed for ^{18}F-FBMARS by incubating the radiotracers with serum at 37°C for up to 4 hours.
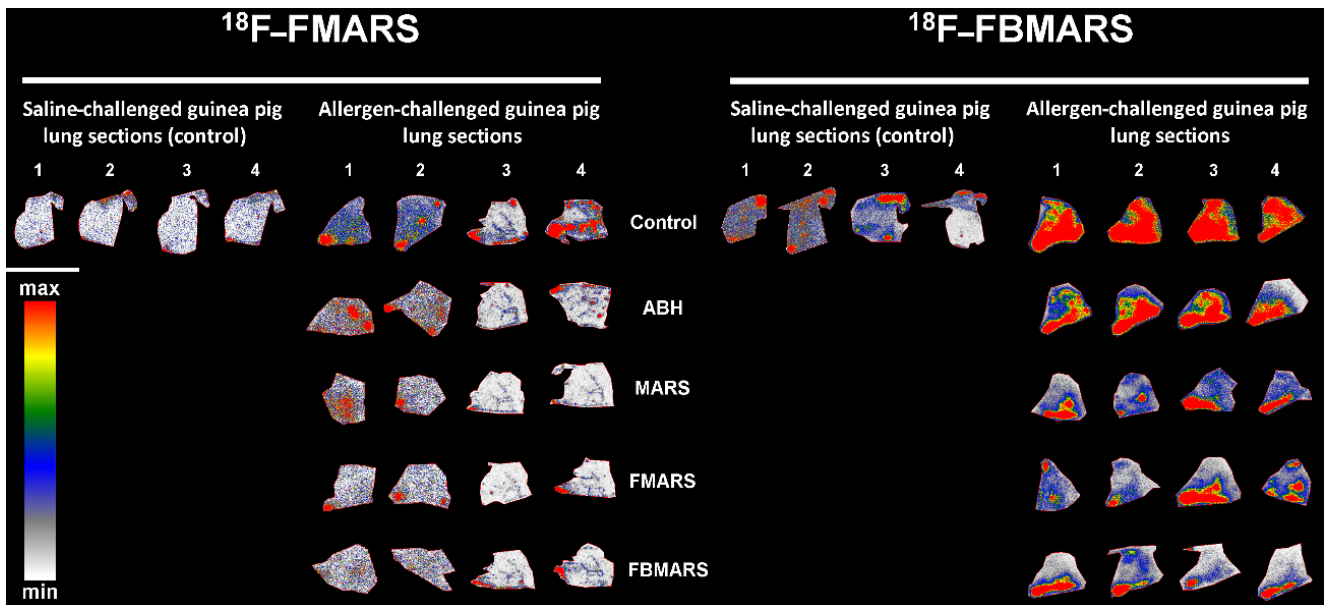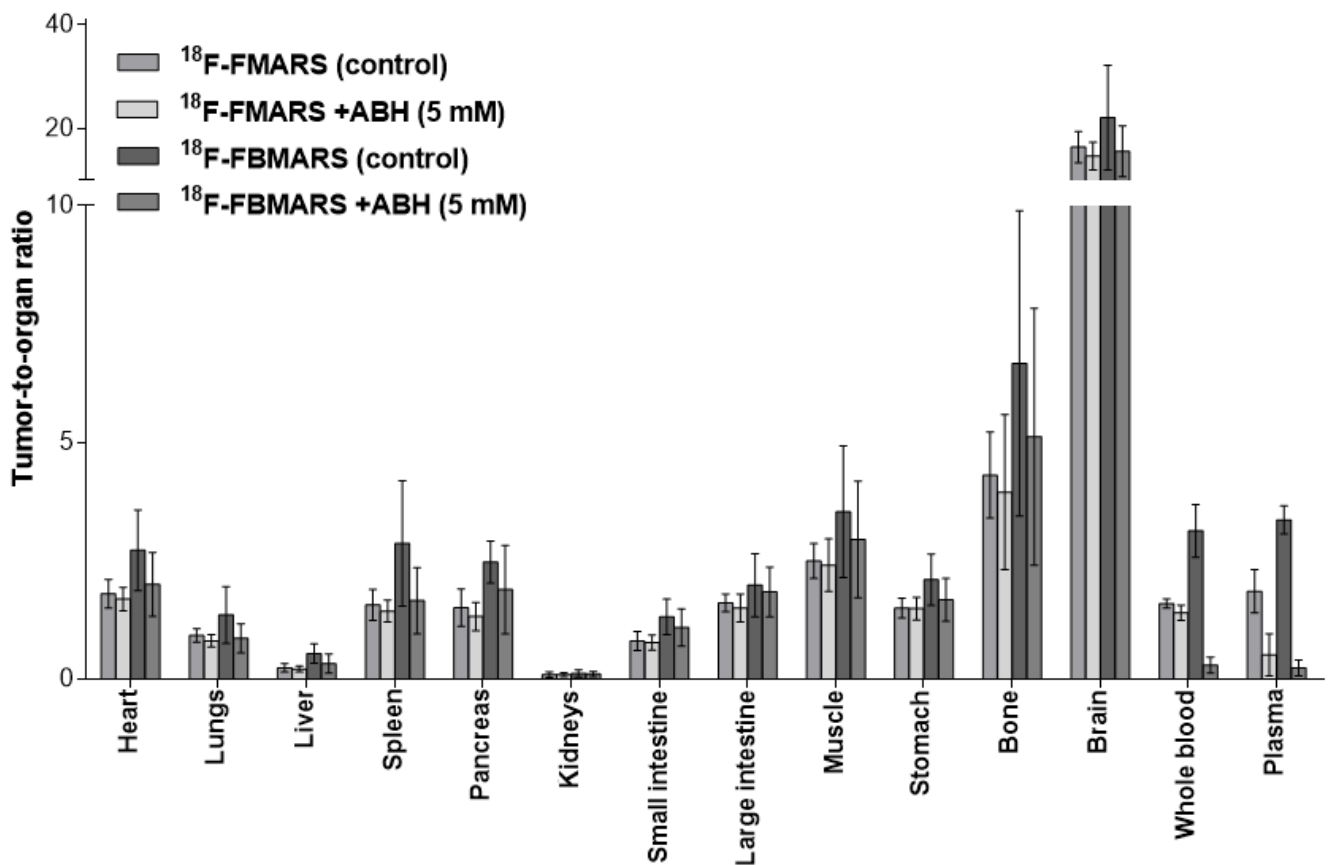

SUPPLEMENTAL FIGURE 8. Representative autoradiography images of saline- and allergen-challenged guinea pig lung sections with ^{18}F-FMARS and ^{18}F-FBMARS without (control) and with competitive arginase inhibition (*n*=4).
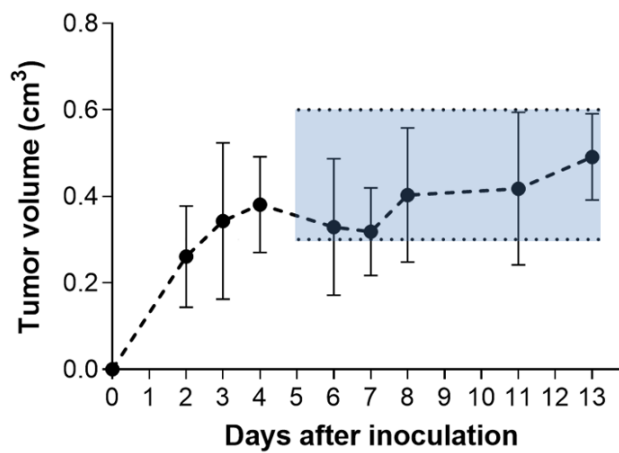

SUPPLEMENTAL FIGURE 9. PC3 solid mass growth after subcutaneous inoculation in mice. The blue area between grid lines represents the ideal tumor volume and moment to perform the PET scan (*n*=32).
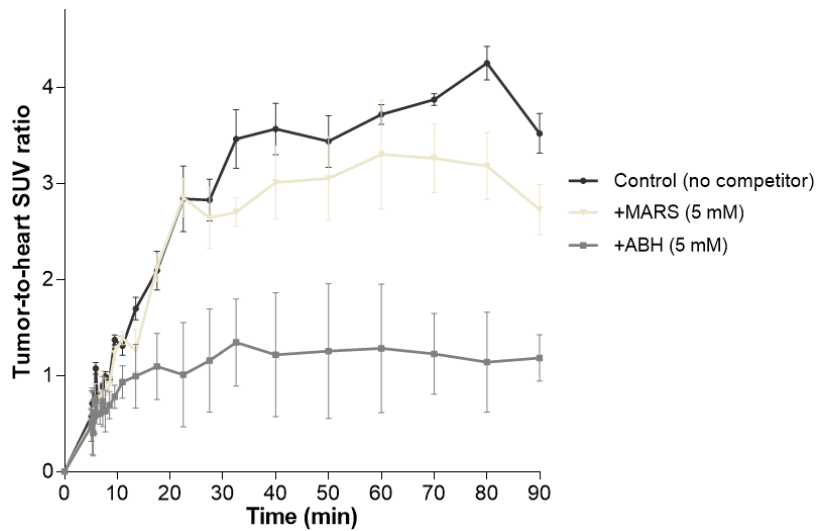
SUPPLEMENTAL FIGURE 10. Tumor-to-blood SUV ratio in the PC3 xenograft mouse model injected with ^{18}F-FBMARS without (control) and with co-injection of the competitive arginase inhibitors ABH and MARS (*n*=3).

**SUPPLEMENTAL FIGURE 11.** Tumor-to-organ ratios of ^{18}F-FMARS (n=7) and ^{18}F-FBMARS (n=9), with and without ABH co-injection, approximately 2 hours after intravenous administration in PC3 xenograft mouse model.
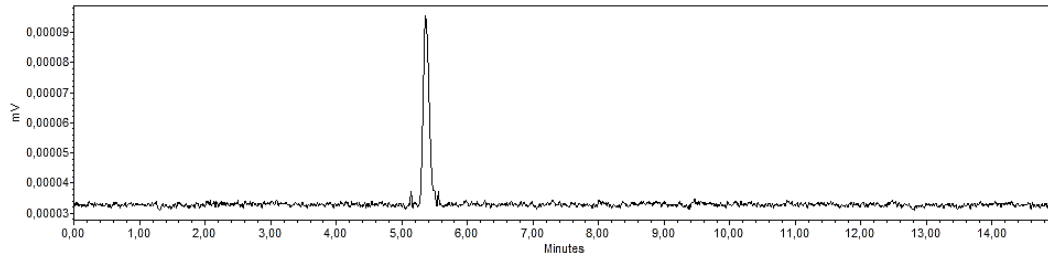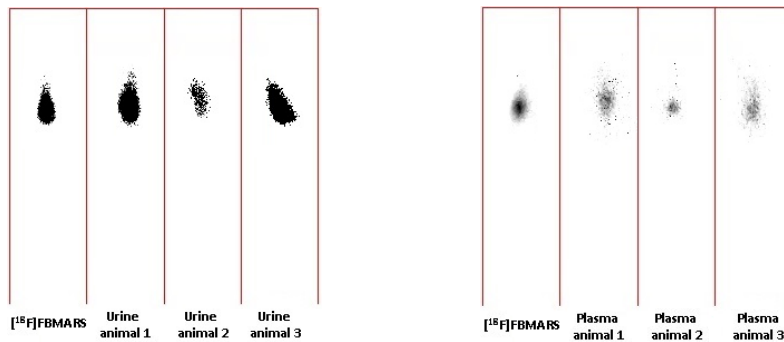
SUPPLEMENTAL FIGURE 12. Representative radio-HPLC of a sample of urine collected approximately 2 hours after ^{18}F-FMARS being intravenously injected in a PC3 xenograft mouse model.
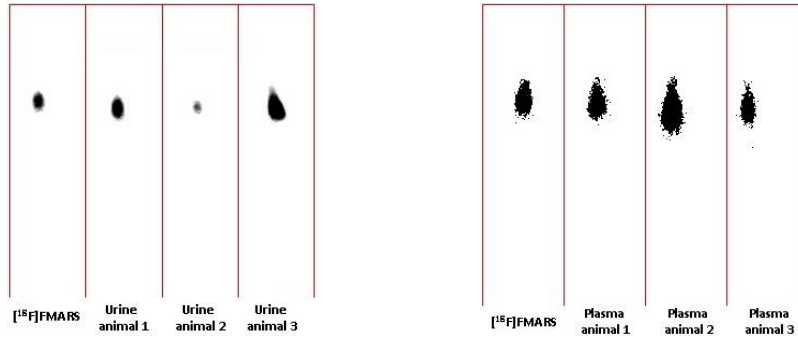
SUPPLEMENTAL FIGURE 13. Representative radio-TLC of samples of urine (left) and plasma (right) collected approximately 2 hours after ^{18}F-FMARS being intravenously injected in a PC3 xenograft mouse model.
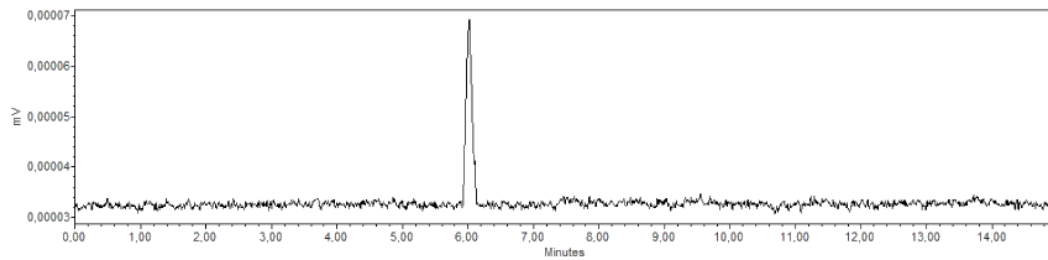
SUPPLEMENTAL FIGURE 14. Representative radio-HPLC of a sample of urine collected approximately 2 hours after ^{18}F-FBMARS being intravenously injected in a PC3 xenograft mouse model.

SUPPLEMENTAL FIGURE 15. Representative radio-TLC of samples of urine (left) and plasma (right) collected approximately 2 hours after ^{18}F-FBMARS being intravenously injected in a PC3 xenograft mouse model.

Supplementary tables

SUPPLEMENTAL TABLE 1

Ex vivo biodistribution of ^{18}F-FMARS and ^{18}F-FBMARS of PC3 xenografted immunocompromised male BALB/c nude mice approximately 2 hours after i.v. radiotracer administration (without/with ABH). Activity in each organ was measured and the percentage of the injected dose (%ID/g) was calculated.

Organs	^{18}F-FMARS (%ID/g)		^{18}F-FBMARS (%ID/g)	
	Control (n=7)	+ABH (5 mM) (n=7)	Control (n=9)	+ABH (5 mM) (n=9)
Heart	0.94 ± 0.48	0.55 ± 0.18	1.33 ± 0.66	0.47 ± 0.25
Lungs	1.82 ± 0.95	1.17 ± 0.41	2.89 ± 1.66	1.10 ± 0.55
Liver	7.15 ± 2.85	4.76 ± 2.22	6.78 ± 3.19	3.38 ± 2.27
Spleen	1.04 ± 0.48	0.64 ± 0.20	1.37 ± 0.71	0.58 ± 0.30
Pancreas	1.10 ± 0.49	0.72 ± 0.26	1.33 ± 0.43	0.53 ± 0.35
Kidneys	22.85 ± 14.2	11.02 ± 4.10	39.14 ± 25.02	11.40 ± 9.48
Small intestine	2.15 ± 1.25	1.21 ± 0.34	2.60 ± 0.89	0.88 ± 0.51
Large intestine	1.03 ± 0.55	0.62 ± 0.18	1.90 ± 1.01	0.48 ± 0.25
Muscle	0.67 ± 0.36	0.39 ± 0.13	1.07 ± 0.54	0.34 ± 0.18
Stomach	1.10 ± 0.55	0.61 ± 0.17	1.65 ± 0.75	0.57 ± 0.36
Bone	0.38 ± 0.19	0.26 ± 0.10	0.60 ± 0.32	0.21 ± 0.16
Brain	0.10 ± 0.05	0.06 ± 0.02	0.18 ± 0.11	0.06 ± 0.03
Tumor (PC3)	1.70 ± 1.00	0.92 ± 0.32	3.23 ± 1.05	0.92 ± 0.58
Whole blood	1.07 ± 0.36	1.91 ± 1.18	1.03 ± 0.61	3.19 ± 1.83
Plasma	0.92 ± 0.46	1.82 ± 1.38	0.96 ± 0.90	4.03 ± 2.54
Urine	250.02 ± 97.45	206.59 ± 73.35	239.87 ± 54.75	168.20 ± 81.33